ISSN 2096-7071 (Print)
ISSN 2097-3101 (Online)
CN 10-1629/R1

CHINA CDC WEEKLY

Vol. 8 No. 29 Jul. 17, 2026

中国疾病预防控制中心周报(英文)

ISSN 2096-7071
9 772096 707262 29>

China CDC Weekly

Editorial Board

Editorial Office

Cover Image: credited from the designer Jiaying Wang.

Perspectives

Caring for Early Pregnancy, Empowering Healthy Beginnings: Strengthening the Health Foundation of Youth Fertility in China on World Population Day 2026

Danan Gu[1,#]

ABSTRACT

Aligning with the 2026 World Population Day theme that emphasizes "Realizing the Hopes and Aspirations of Young People — Today and for the Future," the Chinese national theme specifically focuses on "Caring for Early Pregnancy, Empowering Healthy Beginnings" (*he hu zao yun, guan ai fu neng*) to address declining birth rates. Early pregnancy is the critical golden window for preventing birth defects and mitigating maternal risks, yet historical care models disproportionately focus on later gestational stages. This article examines structural gaps in early pregnancy care, including unequal resource distribution, insufficient mental health services, and limited social support networks. These challenges are closely interconnected and collectively limit the effectiveness, accessibility, and continuity of early pregnancy care. To address these challenges, we propose reconstructing a multidimensional collaborative support network. Key strategies include establishing standardized multidisciplinary clinics, leveraging digital health technologies for equitable access, and integrating medical care with supportive national social policies. Strengthening early pregnancy care through coordinated physiological, psychological, and social support can not only improve pregnancy outcomes but also help alleviate fertility anxiety among young couples, contributing to healthier families and high-quality population dynamics during China's demographic transition.

Introduction: Youth Aspirations and the Imperative of Early Pregnancy Care in a Period of Demographic Transition

July 11, 2026, marks the 37th World Population Day. The United Nations Population Fund (UNFPA) designated the theme as "Realizing the Hopes and Aspirations of Young People — Today and for the Future" (*1*), highlighting the urgency of safeguarding young people's reproductive health and developmental rights amid dramatic global demographic changes (*2*). China adopted the national theme "Caring for Early Pregnancy, Empowering Healthy Beginnings" (*he hu zao yun, guan ai fu neng*) (*3*), directly addressing one of the central issues currently confronting the country's population development.

According to the National Bureau of Statistics of China, the number of births in 2025 was around 7.9 million, marking the fourth consecutive year below 10 million since 2022, while the natural population growth rate remained negative (*4*). Alongside the shrinking number of women of childbearing age and delayed marriage, high housing costs, childcare burdens, and health-related anxieties have become major factors suppressing young people's fertility intentions (*5*). Amidst these challenges, early pregnancy (before 12 weeks of gestation), which represents the initial stage of fetal organogenesis and maternal physiological adaptation (*6*), has acquired renewed significance.

The World Health Organization (WHO) has emphasized that antenatal care is not merely a medical service but also a public health intervention aimed at protecting women's dignity and reproductive rights. However, maternal and child health services in China have historically focused on the second and third trimesters as well as childbirth, while early pregnancy management has remained relatively weak (*7*). The launch of the "Early Pregnancy Care Initiative" in late 2024 by the National Health Commission marked a transition in China's maternal and child health services toward promoting development and quality (*8*). In this context, strengthening early pregnancy care represents not only an important clinical priority but also a strategic opportunity to enhance reproductive health, support young people's reproductive aspirations, and contribute to the development of a fertility-friendly

society.

Vulnerability at the Beginning of Life: The "Golden Window" of Early Pregnancy Health Management

Early pregnancy is the most sensitive and vulnerable stage of embryonic development. From the first day of the last menstrual period to the end of the 12th gestational week, the embryo undergoes critical processes ranging from implantation to the establishment of the primordial structures of major organs (*6*). Health management during this period directly determines pregnancy outcomes and the quality of newborns.

First, early pregnancy represents the "golden window" for primary prevention of birth defects. Neural tube closure occurs between 21 and 28 days after conception, at a time when most women are still unaware of their pregnancy. Landmark studies published in the *New England Journal of Medicine* and subsequent Cochrane systematic reviews have conclusively demonstrated that periconceptional folic acid supplementation significantly reduces the incidence of neural tube defects (*9*). In addition, infections during early pregnancy, such as rubella and cytomegalovirus, as well as exposure to environmental toxins including $PM_{2.5}$ and heavy metals, are high-risk factors for congenital structural abnormalities such as congenital heart disease (*10*).

Second, early pregnancy is the period with the highest incidence of spontaneous miscarriage and ectopic pregnancy (*11*). Approximately 80% of spontaneous miscarriages occur before 12 weeks of gestation, with most associated with chromosomal abnormalities in the embryo (*12–13*). Untreated ectopic pregnancy can directly threaten maternal life (*14*). Therefore, early dynamic monitoring of human chorionic gonadotropin (HCG) levels and ultrasound examinations are not only clinical diagnostic tools but also essential public health measures for reducing reproductive health risks.

The vulnerability of life at its beginning is often exacerbated by insufficient health literacy among young people. Some young women lack awareness regarding preconception folic acid supplementation, teratogenic risks of medications, and environmental protection (*15*). Furthermore, fragmented and misleading information available on the internet has amplified health risks during early pregnancy (*16*). This reality requires a paradigm shift from passive treatment to proactive prevention through earlier health education interventions.

Current Challenges: Key Areas for Improvement in the Transition Toward Comprehensive Reproductive Health Care

Although China has established a nationwide maternal and child health service network, with prenatal examination coverage reaching 98.3% in 2023 (*17*), the early pregnancy care system still needs improvement in several important areas during the transition more holstic and comprehensive reproductive health management (*18*). Unequal healthcare resources constrain timely access to quality services; insufficient psychological support reduces the comprehensiveness of care; and fragmented social support weakens continuity of care beyond the healthcare setting. These challenges are not independent of one another. Rather, they represent interconnected structural barriers operating at the healthcare system, individual, and societal levels. Together, these barriers limit the effectiveness of early pregnancy management and ultimately reduce its potential contribution to improving reproductive health and supporting fertility intentions.

Unequal distribution of primary healthcare resources

High-quality maternal and child healthcare resources remain concentrated in urban areas and the developed regions of eastern China. In some central, western, and rural areas, primary healthcare institutions face shortages of obstetricians and gynecologists, outdated ultrasound equipment, and inadequate genetic counseling services, limiting their capacity to provide systematic early pregnancy risk assessment and intervention (*18–19*). In addition, migrant women often experience interruptions in care during early pregnancy due to difficulties in transferring medical insurance and frequent mobility, creating gaps in the three-tiered birth defect prevention system (*20*).

Beyond disparities in healthcare resources, comprehensive early pregnancy care also requires greater attention to women's psychological well-being. Even where medical services are available, insufficient integration of mental health assessment and counseling may reduce the overall quality and effectiveness of care.

Insufficient integration of mental health support into early pregnancy care Early pregnancy is not only a period of profound physiological change but also a high-risk period for psychological crises. A notable review published in *The Lancet* reported that the

prevalence of non-psychotic perinatal mental disorders, including anxiety and depression, ranges from 10% to 20%, and these conditions are closely associated with preterm birth, low birth weight, and long-term behavioral problems in children (*21*). Biaggi et al. (*22*) further identified lack of social support, economic pressure, and a history of mental illness as key risk factors for antenatal depression.

Currently, most early pregnancy clinics in China still focus primarily on physiological screening and lack standardized psychological assessment tools and professional intervention resources (*23*). When confronted with concerns about career interruption and the financial burden of childrearing, many young women experience psychological distress without sufficient support (*24*).

Psychological well-being during early pregnancy is influenced not only by clinical care but also by the broader social environment. Consequently, improving mental health services alone is insufficient without complementary social policies that reduce the practical and economic pressures associated with childbearing.

Limited coordination between social support networks and the healthcare system Childbearing is not merely a biological process but also a deeply social phenomenon. Young people's fertility anxiety arises not only from fears regarding pregnancy risks but also from concerns about the overall costs of childbirth, parenting, and education (*5*,*23*,*25*). Current early pregnancy care services largely remain confined within the healthcare system and have not been effectively integrated with employment protection, childcare services, and family support policies. The lack of multidimensional social support has made it difficult for the goal of care and empowerment to be fully realized (*26*–*27*).

Strengthening and Expanding: Building a Multidimensional Collaborative Support Network for Early Pregnancy Care

To achieve the goal of "Caring for Early Pregnancy, Empowering Healthy Beginnings," it is necessary to move beyond a purely clinical perspective and establish a multidimensional support network integrating physiological, psychological, and social dimensions.

Promoting standardized early pregnancy clinics and multidisciplinary collaboration Building upon the National Health Commission's ten core messages of the 2024 "Early Pregnancy Care Initiative," China should accelerate the establishment of unified national standards for early pregnancy clinics. Services should expand beyond simple pregnancy confirmation to include high-risk assessment, nutritional counseling, genetic counseling, psychological screening, and post-abortion care. Multidisciplinary collaboration across the departments of obstetrics and gynecology, reproductive endocrinology, psychology, nutrition, and social work should be strengthened to provide comprehensive and compassionate "one-stop" services for young women experiencing unintended pregnancies, high-risk pregnancies, or psychological distress.

Empowering care through digital health technologies Mobile health (mHealth) technologies offer promising solutions for improving the accessibility of early pregnancy care. Recent evidence suggests that digital maternal health interventions, including smartphone applications, teleconsultation, and WeChat-based services, can improve health education, self-management, patient engagement, and communication between pregnant women and healthcare providers while increasing healthcare efficiency (*28*–*29*). China should rely on national maternal and child health information platforms to develop integrated "Internet + Early Pregnancy Care" applications that provide risk alerts, online genetic counseling, psychological self-assessment, and personalized nutritional guidance. Through cross-regional recognition of electronic health records, continuity of care for migrant populations can be strengthened and high-quality healthcare resources can be delivered to primary care institutions through cloud-based systems.

Integrating early pregnancy care into the construction of a fertility-friendly society The ultimate objective of care and empowerment is to alleviate young people's concerns regarding childbearing. Governments, enterprises, and society must work collaboratively. At the policy level, fertility subsidies, universal childcare services, and anti-discrimination mechanisms for women's employment should be strengthened to reduce both explicit and implicit costs of childbearing (*30*). Meanwhile, coordination among health authorities, employers, community organizations, and family support services should be strengthened so that medical care can be seamlessly connected with broader social protection measures throughout early pregnancy. At the community level, early pregnancy care should be incorporated into family health support systems, encouraging partners and family members to participate in pregnancy-related health education and

creating a supportive family-centered environment. Only when society fully respects and institutionally safeguards women's reproductive rights can the medical value of early pregnancy care be transformed into broader social benefits that enhance fertility intentions.

Conclusion

The theme of World Population Day 2026 is not only a macro-level response to global demographic trends but also a reflection of concern for the life planning and well-being of every young individual. As the beginning of human life, early pregnancy directly affects the quality of population development. Specifically, the Chinese national theme "Caring for early pregnancy, empowering healthy beginnings" serves as a timely call to shift the focus from conventional obstetric management toward a more comprehensive model that integrates physiological, psychological, and social support throughout early pregnancy. Such an integrated approach has the potential to improve pregnancy outcomes, reduce fertility-related anxiety, and strengthen the health foundation for future generations. This perspective article aims to stimulate discussion on strengthening early pregnancy care rather than to provide a comprehensive evidence synthesis. Future research should evaluate the effectiveness and cost-effectiveness of multidisciplinary early pregnancy care models, assess the implementation of digital health innovations across diverse settings, and generate more evidence on how integrated healthcare and social support policies can improve reproductive health outcomes and contribute to fertility-friendly societies.

Conflicts of interest: No conflicts of interest.

Disclaimer: Views expressed in the article are solely those of the author and do not necessarily reflect those of the United Nations.

doi: 10.46234/ccdcw2026.146

[#] Corresponding author: Danan Gu, gud@un.org.

[1] Population Division, Department of Economic and Social Affairs, United Nations, New York, NY, USA.

Submitted: July 07, 2026
Accepted: July 10, 2026
Issued: July 17, 2026

REFERENCES

1. United Nations Population Fund. World population day. 2026. https://www.unfpa.org/events/world-population-day. [2026-7-3].
2. UNFPA. State of world population 2024: interwoven lives, threads of hope: ending inequalities in sexual and reproductive health and right. 2024. https://digitallibrary.un.org/record/4045303?v=pdf. [2026-7-3]
3. Health News. 2026 World Population Day China theme determined. 2026. https://www.jkb.com.cn/news/industryNews/2026/0703/512135.html. [2026-7-4]. (In Chinese).
4. National Bureau of Statistics of China. Statistical communiqué of the People's Republic of China on the 2025 national economic and social development. 2026. https://www.stats.gov.cn/sj/zxfb/202602/t20260228_1962662.html. [2026-7-3]. (In Chinese).
5. Liang JZ, Huang WZ, He YF. China Fertility Cost Report 2024. Yuwa Population Research. 2024. https://file.ctrip.com/files/6/yuwa/0R72u12000d9cuimnBF37.pdf. [2026-7-3]. (In Chinese).
6. Cunningham FG, Leveno KJ, Bloom SL, Dashe JS, Hoffman BL, Casey BM, et al. Williams obstetrics. 26th ed. Columbus: McGraw-Hill. 2022.
7. National Health Commission. Maternal safety action improvement plan (2021-2025). 2021. https://www.gov.cn/zhengce/zhengceku/2021-10/15/content_5642740.htm. [2026-7-3]. (In Chinese).
8. National Health Commission. Notice on launching the early pregnancy care action. NHC Maternal and Child Care No. 2024-28. https://www.163.com/dy/article/KGT0N7UD05563I5D.html. [2026-7-3]. (In Chinese).
9. De-Regil LM, Peña-Rosas JP, Fernández-Gaxiola AC, Rayco-Solon P. Effects and safety of periconceptional oral folate supplementation for preventing birth defects. Cochrane Database Syst Rev 2015;2015(12):CD007950. https://doi.org/10.1002/14651858.CD007950.pub3.
10. Stillerman KP, Mattison DR, Giudice LC, Woodruff TJ. Environmental exposures and adverse pregnancy outcomes: a review of the science. Reprod Sci 2008;15(7):631 – 50. https://doi.org/10.1177/1933719108322436.
11. American College of Obstetricians and Gynecologists' (ACOG) Committee on Practice Bulletins—Gynecology. ACOG practice bulletin No. 200: early pregnancy loss. Obstet Gynecol 2018;132(5):e197-207. http://dx.doi.org/10.1097/AOG.0000000000002899.
12. Liu L, Yang YT, Huo HY, Hu N, Wang F. The relationship between fetal tissue chromosomal karyotype and clinical characteristics in patients with spontaneous abortion: a retrospective study. BMC Pregnancy Childbirth 2025;25(1):1043. https://doi.org/10.1186/s12884-025-08106-w.
13. Rai R, Regan L. Recurrent miscarriage. Lancet 2006;368(9535):601 – 11. https://doi.org/10.1016/S0140-6736(06)69204-0.
14. Barnhart KT. Clinical practice. Ectopic pregnancy. N Engl J Med 2009;361(4):379 – 87. https://doi.org/10.1056/NEJMcp0810384.
15. Cui MM, Lu XL, Lyu YY, Wang F, Xie XL, Cheng XY, et al. Knowledge and intake of folic acid to prevent neural tube defects among pregnant women in urban China: a cross-sectional study. BMC Pregnancy Childbirth 2021;21(1):432. https://doi.org/10.1186/s12884-021-03893-4.
16. Neu N, Duchon J, Zachariah P. TORCH infections. Clin Perinatol 2015;42(1):77 – 103. https://doi.org/10.1016/j.clp.2014.11.001.
17. National Health Commission. China Health Statistical Yearbook 2024. Beijing: China Statistics Press; 2025. (In Chinese).
18. Dai Y, Shi XR, Tariq O, Jiang LY, Qu JL, Wei Y, et al. Improving equitable access to antenatal care in China: challenges and potential innovative approaches. China CDC Wkly 2026;8(10):262 – 7. https://doi.org/10.46234/ccdcw2026.042.
19. National Health Commission. Birth defect prevention and control capacity improvement plan (2023-2027). 2023. https://www.nhc.gov.cn/fys/c100078/202308/8230a24d8c8846a9bad6545d7b229162.shtml. [2026-7-3]. (In Chinese).
20. Zhao J, Ding X, Chen YC, Wang F. Analysis on policy practices of hierarchical maternal and child health system in some areas of China.

Chin J Health Policy 2021;14(2):72 – 77. https://doi.org/10.3969/j.issn.1674-2982.2021.02.011.
21. Howard LM, Molyneaux E, Dennis CL, Rochat T, Stein A, Milgrom J. Non-psychotic mental disorders in the perinatal period. Lancet 2014;384(9956):1775 – 1788. https://doi.org/10.1016/S0140-6736(14)61276-9.
22. Biaggi A, Conroy S, Pawlby S, Pariante CM. Identifying the women at risk of antenatal anxiety and depression: a systematic review. J Affect Disord 2016;191:62 – 77. https://doi.org/10.1016/j.jad.2015.11.014.
23. Nisar A, Yin J, Zhang JJ, Qi WL, Yu J, Li JY, et al. Integrating WHO thinking healthy programme for maternal mental health into routine antenatal care in China: a randomized-controlled pilot trial. Front Glob Womens Health 2025;5:1475430. https://doi.org/10.3389/fgwh.2024.1475430.
24. Zhou BW, Wu XC, Ge RX, Zhuo DN. Career women's mental wellbeing in the era of population decline: the effects of working environment and family environment on the mental wellbeing. Front Public Health 2024;12:1462179. https://doi.org/10.3389/fpubh.2024.1462179.
25. Jarosz E, Matysiak A, Osiewalska B. Mothers' parenting behaviours, strain, enjoyment and subsequent childbearing. J Fam Issues 2025;46(5):711 – 32. https://doi.org/10.1177/0192513X241257235.
26. Wu GJ. Further improving policies to build a fertility-friendly society. 2025. https://www.qunzh.com/qzxlk/qz/2025/202519/202510/t20251011_110864.html. [2026-7-3]. (In Chinese).
27. Song DD. The impact of multidimensional intergenerational support on fertility intentions among young Chinese couples: the mediating role of parenting burden and fertility anxiety. Front Psychol 2026;16:1734061. https://doi.org/10.3389/fpsyg.2025.1734061.
28. Li P, Wang HX, Gao X, Han YJ, Wang H, Wang HJ, et al. A randomized controlled trial of weight management based on mobile health technology among overweight or obese pregnant women. J Peking Univ Health Sci 2025;57(3):465 – 72. https://doi.org/10.19723/j.issn.1671-167X.2025.03.009.
29. Xiao J, Li R, Wu YY, Wu T. WeChat-based nursing interventions in women's mobile health: systematic review. JMIR Nurs 2026;9:e82679. https://doi.org/10.2196/82679.
30. Yang JH. Childbirth support and Policyon childbirth support: basic implication and future approach. Shandong Soc Sci 2019;(10):98-107. http://dianda.cqvip.com/Qikan/Article/Detail?id=7003048589. (In Chinese).

Vital Surveillances

Changes in RPV Resistance-Related Mutations Among Antiretroviral Therapy-Naïve HIV-1-Positive Individuals — China, 2004–2023

Xiang Li[1]; Xiu Liu[1]; Peixian Xin[1]; Dong Wang[1]; Jingjing Hao[1]; Chang Song[1]; Jing Hu[1]; Yi Feng[1]; Yuhua Ruan[1]; Hui Xing[1]; Lingjie Liao[1,#]

ABSTRACT

Introduction: Rilpivirine (RPV) is currently included in first-line antiretroviral therapy (ART) regimens in China. However, the baseline RPV resistance remains unclear, especially among different HIV-1 subtypes in China.

Methods: HIV-1 *pol* sequences were collected from ART-naïve HIV-infected individuals between 2004 and 2023. RPV resistance-associated mutations (RAMs) were identified and interpreted using the Stanford HIVdb algorithm. The prevalence of RPV resistance was evaluated over a 20-year study period across different HIV-1 subtypes.

Results: In total, 64,429 HIV-1 *pol* sequences from ART-naïve HIV-infected individuals were included in this analysis. The prevalence of RPV resistance increased significantly from 1.5% (2004–2007) to 3.5% (2020–2023) (P<0.001), which was driven by low-level resistance to RPV. CRF65_cpx (37.7%), CRF55_01B (8.5%), and CRF08_BC (5.0%) showed the highest rates of RPV resistance. In RPV-resistant strains, V179D/E/F/L (43.3%) and E138A/G/K/Q/R (38.0%) were the predominant RAMs. The mutations G190A/C/E/Q/S/T (12.5%) and Y181C/F/I/S/V (11.9%) were also commonly detected. Polymorphic and non-nucleoside reverse transcriptase inhibitor (NNRTI) cross-resistant RAMs were identified in 66.8 and 34.8% of RPV-resistant strains, respectively. The polymorphic mutation V179D/E frequently co-occurred with other RAMs, including E138G (14.4%), K103R (7.8%), and V90I (5.5%), and conferred low- or intermediate-level RPV resistance.

Conclusions: Polymorphic RAMs and NNRTI cross-resistance mutations together account for the increased RPV resistance in China. Additional phenotypic data and clinical research are needed to verify the efficacy of RPV-based ART in patients infected with subtypes CRF65_cpx, CRF55_01B, and CRF08_BC.

Antiretroviral therapy (ART) has improved the prognosis of Human Immunodeficiency Virus (HIV) infection and reduced HIV-related morbidity and mortality. However, the emergence and transmission of HIV drug resistance can undermine ART effectiveness. The prevalence of drug resistance among newly diagnosed ART-naïve HIV-infected adults was 11.4% (*1*). Furthermore, resistance to non-nucleoside reverse transcriptase inhibitors (NNRTIs) was the most prevalent (7.9% of the cases). The prevalence of resistance to the current and former first-line NNRTIs [efavirenz (EFV) and nevirapine (NVP)] has reached 6.5% (*1*).

Rilpivirine (RPV), a second-generation NNRTI, exerts antiviral effects by binding to regions adjacent to the active site of HIV reverse transcriptase (RT), suppressing viral replication. The proportion of treatment-naïve individuals receiving RPV as part of an initial ART regimen increased from 0.04% to 1.3% between 2017 and 2019 (*2*). Owing to its tolerability profile and once-daily dosing, RPV has been included as a first-line ART regimen in China as an alternative to EFV since 2023 (*3*). The baseline data on RPV resistance among ART naïve HIV-infected individuals are scarce, impeding the optimal use of RPV (*4*). The present study aimed to analyze the trend of RPV resistance and characterize RPV resistance-associated mutations (RAMs) among ART-naïve HIV-infected individuals in China from 2004 to 2023 and to provide suggestions for optimizing ART strategies.

METHOD

HIV-1 *pol* sequences were obtained from the local

database of the National Center for AIDS/STD Control and Prevention, China CDC (samples collected between 2004 and 2023) and the HIV Database (https://www.hiv.lanl.gov), as previously described (*5*). All sequences were obtained from ART-naïve HIV-infected adults aged ≥18 years in China. Duplicated sequences, those without sampling year/provincial-level administrative division information, or sequences with mixed bases exceeding 5% of the sequence length were excluded from the study (Supplementary Figure S1, available at https://weekly.chinacdc.cn/). Each sequence covered the coding region for HIV protease (amino acids 10–99) and RT (the first 238 amino acids), corresponding to HXB2 positions 2,280–3,263.

HIV-1 subtypes were determined by phylogenetic analysis using the maximum likelihood method in IQ-Tree (v2.0.7, Integrative Bioinformatics Vienna, Vienna, Austria), with the study sequences aligned with reference sequences retrieved from the HIV gene sequence database (https://nmdc.cn/hiv/tool/sequence). RPV RAMs were identified using the Stanford HIV Drug Resistance Database (http://hivdb.stanford.edu) and interpreted using the HIVdb (v10.1, Stanford University, Stanford, CA, USA). Low, intermediate, and high resistance levels were classified as RPV resistance, whereas potential low-level resistance and susceptibility to RPV were classified as no resistance. RPV RAMs were divided into NNRTI cross-resistance RAMs (conferring low- or higher- level resistance), polymorphic RAMs (conferring potential low-level/even lower resistance and having >1% prevalence in at least one HIV-1 subtype, with the exception of E138G, which confers low-level resistance to RPV), the RPV-specific RAM E138K, and other unclassified RAMs.

The samples were divided into five groups based on the sampling period and the corresponding phases of China's National Free Antiretroviral Treatment Program: 2004–2007, the initial period; 2008–2011, the scale-up period; 2012–2015, the period when the CD4 threshold for ART initiation was elevated to 350 cells/μL; 2016–2019, the universal treatment period regardless of CD4 cell counts; 2020–2023, the recent study period. EFV and NVP remained the core components of the first-line ART regimens throughout the study period and the latter two periods covered the years after the introduction of RPV. The prevalences of RPV resistance and RAMs were evaluated using the chi-square test. Pairwise comparisons between different periods were performed using Bonferroni correction. SAS software (version 9.4; SAS Institute Inc., Cary, NC, USA) was used for statistical analyses. A two-sided $P<0.05$ was considered statistically significant, while a $P<0.005$ indicated significant differences in pairwise comparisons between the two periods.

RESULT

In total, 64,429 sequences (Supplementary Figure S1) from ART-naïve HIV-infected adults in China (2004–2023) were included in the present analysis (Supplementary Table S1, available at https://weekly.chinacdc.cn/). The largest proportion of sequences was obtained from 2012–2015 (33.3%), followed by 2016–2019 (33.2%), 2020–2023 (17.9%), 2008–2011 (13.7%), and 2004–2007 (1.9%). Five predominant HIV-1 subtypes accounted for 94.3% of all the strains [CRF01_AE (38.2%), CRF07_BC (36.5%), CRF08_BC (7.9%), B (7.3%) and CRF55_01B (4.4%)]. A total of 1,538 individuals harbored RPV-resistant strains (overall prevalence rate, 2.4%).

Over the 20-year study period, the prevalence of RPV resistance increased progressively, with rates of 1.5, 1.8, 1.8, 2.6, and 3.5% during 2004–2007, 2008–2011, 2012–2015, 2016–2019, and 2020–2023, respectively ($P<0.001$; Figure 1). Pairwise comparisons revealed statistically significant differences in prevalence between 2012–2015 and 2016–2019 and between 2012–2015 and 2020–2023. The increase in RPV resistance between 2016 and 2023 was primarily attributed to the rising low-level RPV resistance, which increased from 1.2% in 2016–2019 to 2.2% in 2020–2023, with a statistically significant difference between the two periods ($P<0.001$). The prevalence of intermediate-level RPV resistance fluctuated over the 20-year period, peaking at 1.1% during 2016–2019, with significant differences found when compared with periods of 2012–2015 and 2020–2023 ($P<0.001$), whereas high-level RPV resistance remained relatively stable (range, 0.3%–0.5%).

CRF55_01B, CRF08_BC, subtype B, CRF01_AE, and CRF07_BC had RPV resistance prevalences of 8.5%, 5.0%, 3.1%, 1.6%, and 1.5%, respectively (Figure 2A). All five subtypes exhibited an upward trend in RPV resistance during the study period. By 2020–2023, the prevalence of RPV resistance reached 9.3% in CRF55_01B and 7.9% in CRF08_BC.

Additionally, CRF65_cpx showed a high prevalence of RPV resistance (37.7 %), increasing from 33.3% in 2008–2011 to 47.8% in 2020–2023 (Figure 2B).

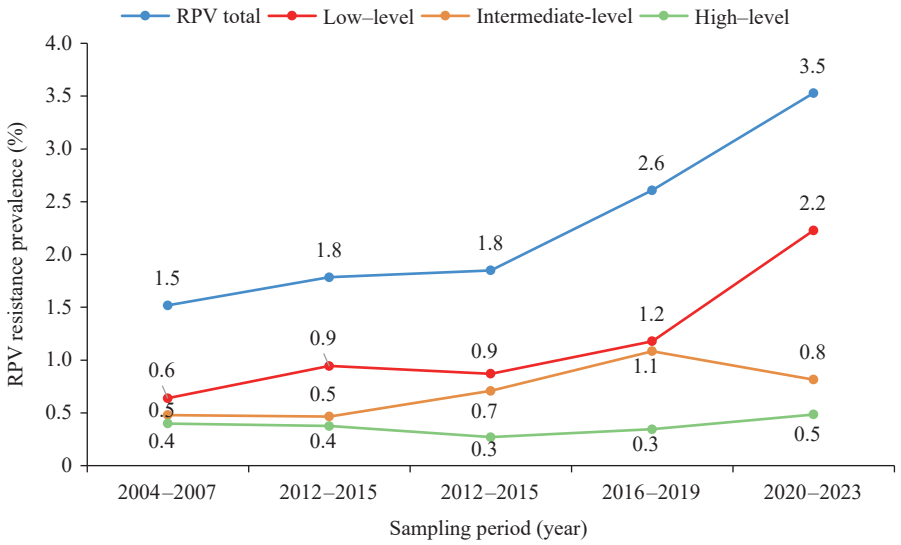

FIGURE 1. The prevalence of RPV resistance among antiretroviral therapy-naïve HIV-infected individuals during the 20-year period in China.
Abbreviation: RPV=rilpivirine; HIV=human immunodeficiency virus; ART=antiretroviral therapy.

Subtype C also exhibited a relatively high RPV resistance rate of 7.0% (31/435), with a rate of 8.8% in 2020–2023.

RPV RAMs were identified at 14 sites within *RT* (Table 1). Among all the HIV strains enrolled, V179D/E/F/L (9.5%) was the most common RPV RAM. Stratified subtype analysis further revealed that these mutations were detected in 95.1% of CRF55_01B isolates and 96.2% of CRF65_cpx isolates, respectively (Supplementary Table S2, available at https://weekly.chinacdc.cn/). Additional RAMs with a prevalence >1% included V106A/I (2.5%), E138A/G/K/Q/R (1.7%), and V90I (1.1%). The remaining RPV RAMs exhibited low prevalence (range, 0.1% to –0.3%). Over the 20-year period, three of the four most common RPV RAMs, V179D/E/F/L, E138A/G/K/Q/R, and V90I, showed an increasing incidence (all $P<0.001$), whereas that of V106A/I decreased ($P<0.001$).

Among the 1,538 strains with RPV resistance, V179D/E/F/L was the most frequent (43.3%), followed by E138A/G/K/Q/R (38.0%), G190A/C/E/Q/S/T (12.5%), and Y181C/F/I/S/V (11.9%; Table 2). Polymorphic RAMs (V90I, A98G, V106I, E138A/G, and V179D/E) were identified in 66.8% of the RPV-resistant strains, whereas NNRTI cross-resistance RAMs (L100I/V, K101E/P, Y181C/F/I/S/V, Y188F/L, G190A/C/E/Q/S, F227C, and M230I/L) were found in 34.8% of RPV-resistant isolates. E138K was only detected in 4.0% of the RPV-resistant strains. Furthermore, polymorphic RAMs were predominant in strains with low-level RPV resistance (80.8%), whereas NNRTI cross-resistance RAMs were present in all strains harboring high-level RPV resistance (100.0%). In RPV resistance strains, V179D/E frequently co-occurred with other mutations [E138G (14.4%), K103R (7.8%), V90I (5.5%), V106I (3.3%), E138A (1.9%), and A98G (1.0%)] which confer low- or intermediate-level RPV resistance. In CRF08_BC, CRF55_01B, and CRF65_cpx, the combinations of V90I with V179D, E138G with V179E, and K103R with V179D accounted for 24.2%, 79.3%, and 93.9% of RPV resistance, respectively (Table 2).

DISCUSSION

In this study, the prevalence of RPV resistance was assessed among 64,429 ART-naïve HIV-infected individuals in China, and a steady increase from 1.5% to 3.5% from 2004 to 2023 was observed. A recent study conducted in southern China reported an RPV resistance rate of 3.4%, consistent with our findings (*6*). A significant increase in RPV resistance prevalence emerged in 2016–2019 following the introduction of RPV in China. However, E138K, the key specific RPV RAM, accounts for <5% of all RPV-resistant strains, suggesting limited clinical application of this drug. Furthermore, E138K did not show an upward temporal trend among resistant isolates (data not shown), indicating that the elevated prevalence of RPV resistance coincides with the clinical usage of RPV in China.

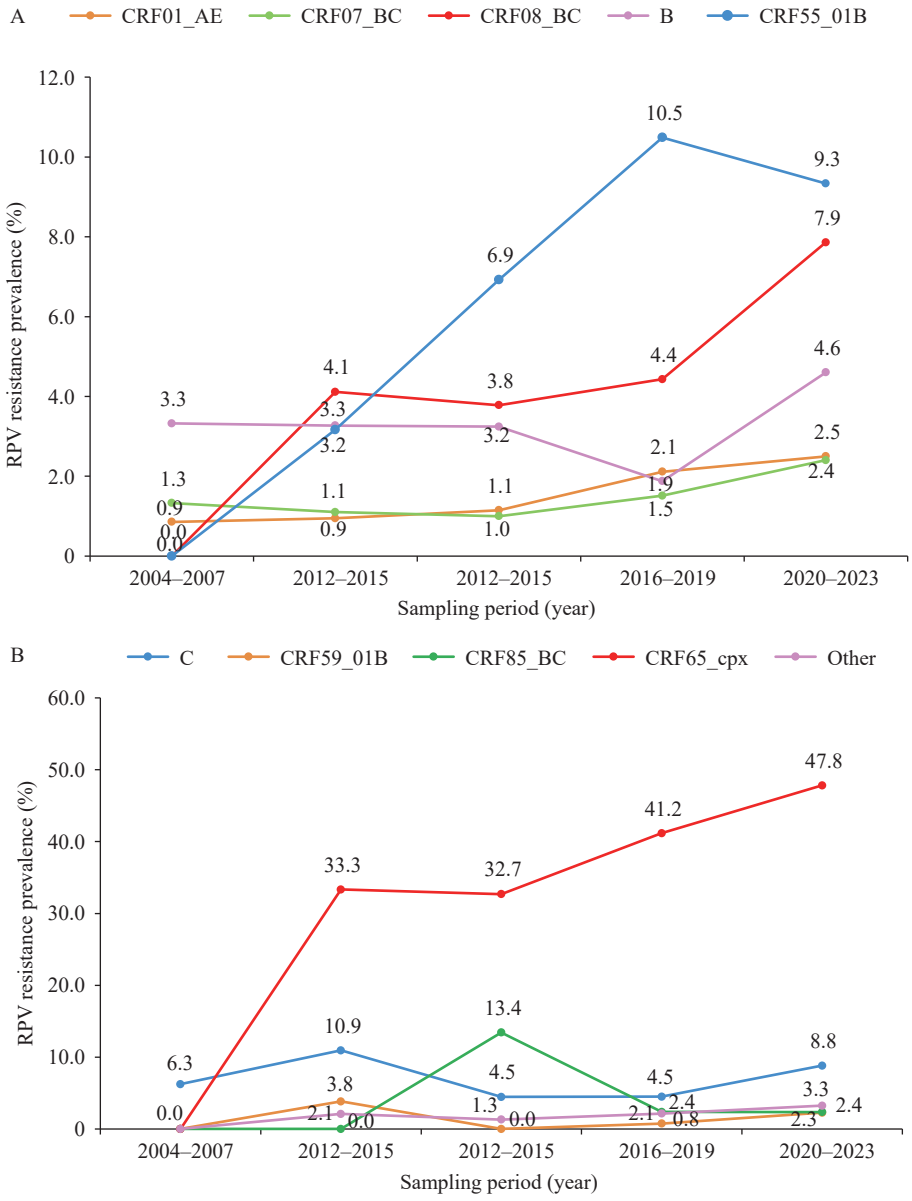

FIGURE 2. The prevalence of RPV resistance in HIV-1 subtypes among antiretroviral therapy-naïve HIV-infected individuals during the 20-year period in China. (A) The prevalence in five major HIV-1 subtypes. (B) The prevalence in HIV-1 subtypes other than the major subtypes.
Abbreviation: RPV=rilpivirine; HIV=human immunodeficiency virus.

In 2020–2023 CRF08_BC and CRF55_01B exhibited RPV resistance rates close to 10%, whereas, CRF65_cpx had a resistance prevalence of <50%. This uneven distribution across subtypes may be attributed to inherent differences in the *RT* genes. E138A (*7*) is most prevalent in subtypes C (6.1%), F (5.1%), and A (3.3%). In this study, E138A was observed at a much higher frequency in CRF08_BC (7.8%) than in other subtypes. The contribution of this mutation to ART failure remains debatable (*8*), and it has been reclassified as a RAM, conferring potential low-level resistance to RPV.

RPV resistance observed in this study likely reflects the combined effects of natural polymorphisms and cross-resistance to other NNRTIs. V179D and V179E were the most prevalent mutations at V179 (99.9%). Neither mutation confers low-, intermediate-, or high-level RPV resistance; however, either mutation can do so when co-occuring with other RT RAMs. V179D/E prevalence increased gradually over the 20-year study period and exceeded 10% among the prevailing HIV-1 strains in China (2020–2023). Additionally, V179E and V179D were identified as inherent amino acid polymorphisms in CRF55_01B and CRF65_cpx,

TABLE 1. The prevalence of RPV resistance-associated mutations among ART-naïve HIV-infected individuals during the 20-year period in China.

Drug resistance mutation	2004–2007 (*N*=1,251) *n*[§] (%)[¶]	2008–2011 (*N*=8,795) *n* (%)	2012–2015 (N=21,461) *n* (%)	2016–2019 (*N*=21,389) *n* (%)	2020–2023 (*N*=11,533) *n* (%)	*P**	Total (*N*=64,429) *n* (%)
V90I	13 (1.0)	111 (1.3)	150 (0.7)	185 (0.9)	250 (2.2)	<0.0001	709 (1.1)
A98G	2 (0.2)	17 (0.2)	15 (0.1)	30 (0.1)	43 (0.4)	0.001	107 (0.2)
L100I/V	1 (0.1)	2 (0)	4 (0)	6 (0)	7 (0.1)	0.201	20 (0)
K101E/H/P	1 (0.1)	17 (0.2)	40 (0.2)	45 (0.2)	42 (0.4)	0.003	145 (0.2)
K103R[†]	23 (1.8)	194 (2.2)	533 (2.5)	487 (2.3)	356 (3.1)	<0.0001	1,593 (2.5)
V106A/I	42 (3.4)	340 (3.9)	589 (2.7)	436 (2.0)	220 (1.9)	<0.0001	1,627 (2.5)
V108I	5 (0.4)	26 (0.3)	51 (0.2)	37 (0.2)	32 (0.3)	0.300	151 (0.2)
E138A/G/K/Q/R	22 (1.8)	117 (1.3)	296 (1.4)	416 (1.9)	271 (2.3)	<0.0001	1,122 (1.7)
V179D/E/F/L	34 (2.7)	539 (6.1)	2,038 (9.5)	2,340 (10.9)	1,189 (10.3)	<0.0001	6,140 (9.5)
Y181C/F/I/S/V	7 (0.6)	27 (0.3)	53 (0.2)	62 (0.3)	34 (0.3)	0.701	183 (0.3)
Y188F/L	0 (0)	10 (0.1)	8 (0)	8 (0)	12 (0.1)	0.691	38 (0.1)
G190A/C/E/Q/S/T/V	3 (0.2)	22 (0.3)	51 (0.2)	69 (0.3)	48 (0.4)	0.007	193 (0.3)
H221Y	1 (0.1)	10 (0.1)	23 (0.1)	39 (0.2)	12 (0.1)	0.430	85 (0.1)
F227C/L/Y	3 (0.2)	6 (0.1)	20 (0.1)	43 (0.2)	11 (0.1)	0.258	83 (0.1)
M230I/L	2 (0.2)	4 (0)	7 (0)	25 (0.1)	5 (0)	0.457	43 (0.1)

Abbreviation: HIV=human immunodeficiency virus; ART=antiretroviral therapy; RPV=rilpivirine.
* *P* refers to Pearson's chi-square test. *P*<0.05 is statistically significant.
[†] K103R is not a typical RPV resistance-associated mutation, and this mutation alone cannot reduce susceptibility to rilpivirine.
[§] Number of RPV resistance-associated mutations in ART-naïve individuals
[¶] The detection rate of RPV resistance-associated mutations in ART-naïve individuals infected with HIV.

respectively (*9*). V179D/E compromises the efficacy of NNRTI-containing regimens either during the first year of ART or in patients with a baseline viral load of at least 100,000 copies/mL (*10–11*).

According to a national cross-sectional molecular epidemiological survey (2018), CRF01_AE and CRF07_BC together accounted for 76.6% of all HIV-1 strains in China. CRF08_BC and CRF55_01B accounted for 9.0% and 3.9%, respectively, whereas CRF65_cpx accounted for <0.5%. These three subtypes accounted for approximately 14% of all the HIV-1 strains. Despite their relatively low prevalence, these subtypes are concentrated in southern/southwestern China (*12–14*), regions characterized by frequent population mobility and a historically high proportion of people living with HIV. Caution should be exercised in these regions when incorporating RPV into ART regimens. Further phenotypic and clinical investigations are required to clarify the impact of RPV-based ART in patients infected with the CRF55_01B and CRF65_cpx HIV-1 strains.

Although K103N, the most common RAM linked to EFV, did not confer resistance to RPV, cross-resistance between RPV and EFV and/or NVP was common. This finding was likely due to RAMs at positions Y181, G190, and K101, consistent with previous studies (*15*). Among these, Y181C and G190A were the most frequent. Furthermore, they confer high-level resistance to RPV when combined with K101E. Accordingly, RPV-containing regimens are not recommended as salvage therapies following the failure of EFV-based ART (*16*).

This study has several strengths, including a large number of HIV-1 sequences, long surveillance duration, and nationwide coverage of ART-naïve HIV-infected adults in China, yielding robust data on RPV resistance dynamics. However, this study has some limitations. First, the study relied on retrospective molecular surveillance data, which might have had a sampling bias. The prevalence of HIV-1 subtype B in this study was approximately 10% higher than that reported in a national cross-sectional survey in 2006 (*17*). Because subtype B exhibited higher RPV resistance rates than the other four subtypes during that period, the prevalence of RPV resistance in the early years was likely overestimated. However, this bias would not alter the overall increasing trend of RPV resistance between 2004 and 2023. Second, the temporal trend in RPV resistance could be confounded by changes in population composition over the study

TABLE 2. The prevalence of RPV resistance-associated mutations in RPV-resistance isolates among different HIV-1 subtypes during the 20-year period in China.

Drug resistance mutation	CRF01_AE (*N*=394) *n*** (%††)	CRF07_BC (*N*=352) *n* (%)	CRF08_BC (*N*=256) *n* (%)	CRF55_01B (*N*=237) *n* (%)	B (*N*=147) *n* (%)	C (*N*=31) *n* (%)	CRF65_cpx (*N*=49) *n* (%)	Others (*N*=72) *n* (%)	Total (*N*=1,538) *n* (%)
V90I	14 (3.6)	21 (6.0)	77 (30.1)	11 (4.6)	8 (5.4)	1 (3.2)	0 (0)	1 (1.4)	133 (8.6)
A98G	34 (8.6)	24 (6.8)	6 (2.3)	12 (5.1)	6 (4.1)	15 (48.4)	0 (0)	10 (13.9)	107 (7.0)
L100I/V	6 (1.5)	5 (1.4)	5 (2.0)	0 (0)	5 (3.4)	0 (0)	0 (0)	0 (0)	21 (1.4)
K101E/H/P	54 (13.7)	45 (12.8)	16 (6.3)	1 (0.4)	13 (8.8)	5 (16.1)	0 (0)	8 (11.1)	142 (9.2)
K103R	73 (18.5)	28 (8.0)	9 (3.5)	1 (0.4)	8 (5.4)	6 (19.4)	46 (93.9)	13 (18.1)	184 (12.0)
V106A/I	39 (9.9)	2 (0.6)	25 (9.8)	8 (3.4)	42 (28.6)	2 (6.5)	1 (2.0)	2 (2.8)	121 (7.9)
V108I	12 (3.0)	3 (0.9)	5 (2.0)	6 (2.5)	5 (3.4)	0 (0)	0 (0)	3 (4.2)	34 (2.2)
E138A/G/K/Q/R	63 (16.0)	176 (50.0)	93 (36.3)	194 (81.9)	34 (23.1)	4 (12.9)	2 (4.1)	19 (26.4)	585 (38.0)
V179D/E/F/L	122 (31.0)	60 (17.0)	125 (48.8)	235 (99.2)	41 (27.9)	9 (29.0)	49 (100.0)	25 (34.7)	666 (43.3)
Y181C/F/I/S/V	74 (18.8)	35 (9.9)	5 (2.0)	5 (2.1)	33 (22.4)	4 (12.9)	0 (0)	22 (30.6)	178 (11.6)
Y188F/L	6 (1.5)	14 (4.0)	3 (1.2)	1 (0.4)	18 (12.2)	0 (0)	0 (0)	1 (1.4)	43 (2.8)
G190A/C/E/Q/S/T/V	108 (27.4)	33 (9.4)	9 (3.5)	2 (0.8)	29 (19.7)	2 (6.5)	0 (0)	9 (12.5)	192 (12.5)
H221Y	14 (3.6)	4 (1.1)	5 (2.0)	3 (1.3)	18 (12.2)	0 (0)	0 (0)	4 (5.6)	48 (3.1)
F227C/L/Y	13 (3.3)	7 (2.0)	42 (16.4)	0 (0)	4 (2.7)	0 (0)	0 (0)	3 (4.2)	69 (4.5)
M230I/L	19 (4.8)	12 (3.4)	3 (1.2)	2 (0.8)	7 (4.8)	0 (0)	0 (0)	0 (0)	43 (2.8)
Categories of RPV RAMs									
NNRTI cross-resistance RAMs*	220 (55.8)	130 (36.9)	41 (16.0)	11 (4.6)	90 (61.2)	10 (32.3)	0 (0)	33 (45.8)	535(34.8)
Polymorphic RAMs†	200 (50.8)	232 (65.9)	166 (64.8)	236 (99.6)	77 (52.4)	26 (83.9)	49 (100.0)	41 (56.9)	1027(66.8)
RPV-specific RAM§	18 (4.6)	16 (4.6)	19 (7.4)	1 (0.4)	7 (4.8)	0 (0)	0 (0)	0 (0)	61(4.0)
Others¶	50 (12.7)	17 (4.8)	72 (28.1)	9 (3.8)	31 (21.1)	0 (0)	0 (0)	19 (26.4)	198(12.9)
Most frequent RAM combinations involving V179									
V90I, V179DE	5 (1.3)	5 (1.4)	62 (24.2)	9 (3.8)	2 (1.4)	1 (3.2)	0 (0)	0 (0)	84 (5.5)
A98G, V179DE	0 (0)	2 (0.6)	1 (0.4)	12 (5.1)	0 (0)	0 (0)	0 (0)	1 (1.4)	16 (1.0)
K103R, V179DE	47 (11.9)	11 (3.1)	4 (1.6)	0 (0)	0 (0)	3 (9.7)	46 (93.9)	9 (12.5)	120 (7.8)
V106I, V179DE	20 (5.1)	0 (0)	8 (3.1)	6 (2.5)	13 (8.8)	2 (6.5)	1 (2.0)	1 (1.4)	51 (3.3)
E138A, V179DE	0 (0)	4 (1.1)	20 (7.8)	0 (0)	0 (0)	2 (6.5)	1 (2.0)	2 (2.8)	29 (1.9)
E138G, V179DE	5 (1.3)	10 (2.8)	9 (3.5)	188 (79.3)	8 (5.4)	0 (0)	1 (2.0)	1 (1.4)	222 (14.4)

Abbreviation: HIV=human immunodeficiency virus; ART=antiretroviral therapy; RPV=rilpivirine; NNRTI=non-nucleoside reverse transcriptase inhibitor; RAM=resistance-associated mutation.

* NNRTI cross-resistance RAMs include L100I/V, K101E/P, Y181C/F/I/S/V, Y188F/L, G190A/C/E/Q/S, F227C, and M230I/L.

† Polymorphic RAMs include V90I, A98G, V106I, E138A/G, and V179D/E.

§ RPV-specific RAM refers to E138K; this mutation is one of the E138A/G/K/Q/R mutations, along with E138A, E138G, E138Q, and E138R.

¶ Other RPV-RAMs include K101H, V106A, V108I, E138Q/R, V179F/L, G190T/V, H221Y, and F227L/Y.

** Number of RPV-associated drug resistance mutations in RPV resistance isolates among different HIV-1 subtypes.

†† The detection rate of RPV-associated drug resistance mutations in RPV resistance isolates among different HIV-1 subtypes.

period, including shifts in the distribution of HIV-1 subtypes, transmission routes, and demographic characteristics of the tested populations. However, owing to missing data on patient demographic characteristics, the potential correlations between these factors and RPV resistance were not assessed. Third, the phenotypic effect of RPV RAMs on HIV-1 strains prevalent in China was not validated. Thus, further studies are required to provide evidence-based implications for clinical decision-making.

In conclusion, the prevalence of RPV resistance increased significantly and was mostly driven by low-level RPV resistance. Polymorphic RAMs and NNRTI cross-resistance mutations collectively contribute to increased RPV resistance. Continuous molecular surveillance is crucial for monitoring the evolving RPV resistance trends and identifying emerging and circulating resistant strains. Moreover, caution is

warranted when prescribing RPV-containing regimens to patients infected with HIV-1 strains with high RPV resistance prevalence.

Conflicts of interest: No conflicts of interest.

Ethical statement: Approved by the Ethics Committee of the National Center for AIDS/STD Control and Prevention (Approval No: X140617334).

Funding: Supported by the National Science and Technology Major Project-National Mega Project on Major Infectious Disease Prevention (2025ZD01904705).

doi: 10.46234/ccdcw2026.147

[#] Corresponding author: Lingjie Liao, liaolj@chinaaids.cn.

[1] National Key Laboratory of Intelligent Tracking and Forecasting for Infectious Diseases, National Center for AIDS/STD Control and Prevention (NCAIDS), Chinese Center for Disease Control and Prevention & Chinese Academy of Preventive Medicine, Beijing, China.

Submitted: March 30, 2026
Accepted: June 24, 2026
Issued: July 17, 2026

REFERENCES

1. Hao JJ, Liu X, Wang D, Hu HP, Li FY, Li YT, et al. Transmitted HIV-1 drug resistance among newly diagnosed individuals in 31 provincial-level administrative divisions in China in 2023: a cross-sectional survey. Clin Infect Dis 2025;81(3):531 – 8. https://doi.org/10.1093/cid/ciaf159.
2. Wu XS, Wu GH, Ma P, Wang RG, Li LH, Chen YY, et al. Associations of modern initial antiretroviral therapy regimens with all-cause mortality in people living with HIV in resource-limited settings: a retrospective multicenter cohort study in China. Nat Commun 2023;14(1):5334. https://doi.org/10.1038/s41467-023-41051-w.
3. Xie ZY, Duan ZZ. Evolving Challenges in the Implementation of China's "Four Frees and One Care" Policy for HIV/AIDS. Risk Manag Healthc Policy. 2024;17:1315-21. https://dx.doi.org/10.2147/RMHP.S459173
4. Theys K, Van Laethem K, Gomes P, Baele G, Pineda-Peña AC, Vandamme AM, et al. Sub-epidemics explain localized high prevalence of reduced susceptibility to rilpivirine in treatment-naive HIV-1-infected patients: subtype and geographic compartmentalization of baseline resistance mutations. AIDS Res Hum Retroviruses 2016;32(5):427 – 33. https://doi.org/10.1089/aid.2015.0095.
5. Liu X, Wang D, Hu J, Song C, Liao LJ, Feng Y, et al. Changes in HIV-1 subtypes/sub-subtypes, and transmitted drug resistance among ART-Naïve HIV-infected individuals — China, 2004-2022. China CDC Wkly 2023;5(30):664 – 71. https://doi.org/10.46234/ccdcw2023.129.
6. Lv SY, Lan Y, He YZ, Li QM, Ling XM, Li JB, et al. Pretreatment drug resistance among people living with HIV from 2018 to 2022 in Guangzhou, China. J Med Virol 2024;96(10):e29937. https://doi.org/10.1002/jmv.29937.
7. Calvez V, Marcelin AG, Vingerhoets J, Hill A, Hadacek B, Moecklinghoff C. Systematic review to determine the prevalence of transmitted drug resistance mutations to rilpivirine in HIV-infected treatment-naive persons. Antivir Ther 2016;21(5):405 – 12. https://doi.org/10.3851/IMP3024.
8. Maruapula D, Moraka NO, Bareng OT, Mokgethi PT, Choga WT, Seatla KK, et al. Archived rilpivirine-associated resistance mutations among ART-naive and virologically suppressed people living with HIV-1 subtype C in Botswana: implications for cabotegravir/rilpivirine use. J Antimicrob Chemother 2023;78(10):2489 – 95. https://doi.org/10.1093/jac/dkad258.
9. Liu YJ, Li HP, Wang XL, Han JW, Jia L, Li TY, et al. Natural presence of V179E and rising prevalence of E138G in HIV-1 reverse transcriptase in CRF55_01B viruses. Infect Genet Evol 2020;77:104098. https://doi.org/10.1016/j.meegid.2019.104098.
10. Lv SY, Lan Y, Li QM, Ling XM, Li JB, Wen CY, et al. Impact of V179D/E mutations on antiretroviral therapy outcomes in people living with HIV-1: a 3-year retrospective study. Front Cell Infect Microbiol 2025;15:1691715. https://doi.org/10.3389/fcimb.2025.1691715.
11. Wang ZY, Zhang M, Wang JR, Liu L, Chen J, Zhang RF, et al. Efficacy of efavirenz-based regimen in Antiretroviral-Naïve patients with HIV-1 V179D/E mutations in Shanghai, China. Infect Dis Ther 2023;12(1):245 – 55. https://doi.org/10.1007/s40121-022-00723-8.
12. Li XG, Trovão NS. The evolutionary and transmission dynamics of HIV-1 CRF08_BC. PLoS One 2024;19(9):e0310027. https://doi.org/10.1371/journal.pone.0310027.
13. Gan MZ, Zheng S, Hao JJ, Ruan YH, Liao LJ, Shao YM, et al. The prevalence of CRF55_01B among HIV-1 strain and its connection with traffic development in China. Emerg Microbes Infect 2021;10(1):256 – 65. https://doi.org/10.1080/22221751.2021.1884004.
14. Liu YJ, Gui T, Jia L, Li L, Bao ZY, Li HP, et al. Phylogenetic analysis of HIV-1 CRF65_CPX reveals yunnan province is still a source contributing to the spread of HIV-1 in China. JAIDS J Acquir Immune Defic Syndr 2015;70(3):e120 – 2. https://doi.org/10.1097/QAI.0000000000000775.
15. Diphoko T, Gaseitsiwe S, Kasvosve I, Moyo S, Okatch H, Musonda R, et al. Prevalence of Rilpivirine and Etravirine Resistance Mutations in HIV-1 Subtype C-Infected Patients Failing Nevirapine or Efavirenz-Based Combination Antiretroviral Therapy in Botswana. AIDS Res Hum Retroviruses. 2018;34(8):667-71. http://dx.doi.org/10.1089/AID.2017.0135
16. Gouissi Anguechia DH, Bouba Y, Semengue ENJ, Takou D, Chenwi CA, Mekel VK, et al. HIV-1 cross-resistance to second-generation non-nucleoside reverse transcriptase inhibitors among individuals failing antiretroviral therapy in Cameroon: implications for the use of long-acting treatment regimens in low- and middle-income countries. JAC-Antimicrob Resist 2025;7(2):dlaf059. https://doi.org/10.1093/jacamr/dlaf059.
17. He X, Xing H, Ruan YH, Hong KX, Cheng CL, Hu YY, et al. A comprehensive mapping of HIV-1 genotypes in various risk groups and regions across China based on a nationwide molecular epidemiologic survey. PLoS One 2012;7(10):e47289. https://doi.org/10.1371/journal.pone.0047289.

SUPPLEMENTARY MATERIAL

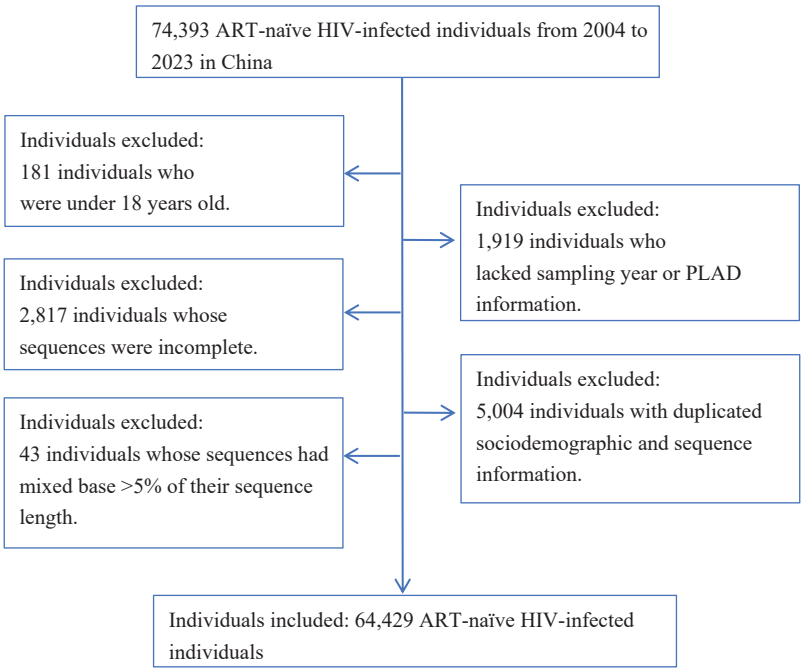

SUPPLEMENTARY FIGURE S1. Inclusion criteria for study subjects.
Abbreviation: RPV=rilpivirine; HIV=human immunodeficiency virus; ART=antiretroviral therapy, PLAD=provincial-level administrative division.

SUPPLEMENTARY TABLE S1. Distribution of HIV-1 subtypes among ART-naïve HIV-infected individuals during the 20-year period in China.

HIV-1 subtypes	2004–2007		2008–2011		2012–2015		2016–2019		2020–2023		Total	
	*n**	Proportion (%)†	*n*	Proportion (%)	*n*	Proportion (%)	*n*	Proportion (%)	*n*	Proportion (%)	*n*	Proportion (%)
Total	1,251	100.0	8,795	100.0	21,461	100.0	21,389	100.0	11,533	100.0	64,429	100.0
CRF01_AE	467	37.3	3,912	44.5	9,048	42.2	7,906	37.0	3,280	28.4	24,613	38.2
CRF07_BC	301	24.1	2,540	28.9	7,402	34.5	8,193	38.3	5,077	44.0	23,513	36.5
CRF08_BC	144	11.5	389	4.4	1,190	5.5	2,099	9.8	1,298	11.3	5,120	7.9
B	301	24.1	1,223	13.9	1,634	7.6	959	4.5	565	4.9	4,682	7.3
CRF55_01B	1	0.1	221	2.5	1,170	5.5	1,125	5.3	332	2.9	2,849	4.4
C	16	1.3	128	1.5	112	0.5	111	0.5	68	0.6	435	0.7
CRF85_BC	0	0	0	0	67	0.3	84	0.4	170	1.5	321	0.5
CRF59_01B	2	0.2	26	0.3	100	0.5	132	0.6	44	0.4	304	0.5
CRF79_0107	0	0	19	0.2	47	0.2	66	0.3	62	0.5	194	0.3
CRF65_cpx	0	0	21	0.2	52	0.2	34	0.2	23	0.2	130	0.2
Others	21	1.7	342	3.9	739	3.4	812	3.8	658	5.7	2,572	4.0

Abbreviation: HIV=human immunodeficiency virus; ART=antiretroviral therapy.
* Number of ART-naïve individuals infected with different HIV-1 subtypes.
† The proportion of ART-naïve individuals infected with different HIV-1 subtypes.

SUPPLEMENTARY TABLE S2. The prevalence of RPV resistance-associated mutations among different HIV-1 subtypes during 20-year period in China.

Drug resistance mutation	CRF01_AE (*N*=24,613) *n** (%†)	CRF07_BC (*N*=23,513) *n* (%)	CRF08_BC (N=5,120) *n* (%)	CRF55_01B (*N*=2,849) *n* (%)	B (*N*=4,682) *n* (%)	C (*N*=435) *n* (%)	CRF65_cpx (*N*=130) *n* (%)	Others (*N*=3,807) *n* (%)
V90I	116 (0.5)	157 (0.7)	279 (5.4)	11 (0.4)	83 (1.8)	22 (5.1)	0 (0)	41 (1.3)
A98G	34 (0.1)	24 (0.1)	6 (0.1)	12 (0.4)	6 (0.1)	15 (3.4)	0 (0)	10 (0.3)
L100I/V	6 (0)	5 (0)	5 (0.1)	0 (0)	5 (0.1)	0 (0)	0 (0)	0 (0)
K101E/H/P	54 (0.2)	48 (0.2)	16 (0.3)	1 (0)	13 (0.3)	5 (1.1)	0 (0)	8 (0.3)
K103R	853 (3.5)	314 (1.3)	60 (1.2)	28 (1.0)	151 (3.2)	14 (3.2)	47 (36.2)	126 (4.1)
V106A/I	522 (2.1)	27 (0.1)	123 (2.4)	21 (0.7)	842 (18.0)	3 (0.7)	1 (0.8)	88 (2.9)
V108I	64 (0.3)	25 (0.1)	21 (0.4)	6 (0.2)	27 (0.6)	0 (0)	0 (0)	8 (0.3)
E138A/G/K/Q/R	105 (0.4)	228 (1.0)	460 (9.0)	194 (6.8)	50 (1.1)	14 (3.2)	2 (1.5)	69 (2.2)
V179D/E/F/L	1,310 (5.3)	900 (3.8)	524 (10.2)	2,709 (95.1)	306 (6.5)	31 (7.1)	125 (96.2)	239 (7.7)
Y181C/F/I/S/V	74 (0.3)	35 (0.1)	5 (0.1)	5 (0.2)	33 (0.7)	4 (0.9)	0 (0)	22 (0.7)
Y188F/L	6 (0)	14 (0.1)	3 (0.1)	1 (0)	18 (0.4)	0 (0)	0 (0)	1 (0)
G190A/C/E/Q/S/T/V	108 (0.4)	34 (0.1)	9 (0.2)	2 (0.1)	29 (0.6)	2 (0.5)	0 (0)	9 (0.3)
H221Y	29 (0.1)	14 (0.1)	14 (0.3)	3 (0.1)	18 (0.4)	1 (0.2)	0 (0)	6 (0.2)
F227C/L/Y	19 (0.1)	12 (0.1)	42 (0.8)	0 (0)	5 (0.1)	0 (0)	0 (0)	4 (0.1)
M230I/L	19 (0.1)	12 (0.1)	3 (0.1)	2 (0.1)	7 (0.1)	0 (0)	0 (0)	0 (0)

Abbreviation: HIV=human immunodeficiency virus; RPV=rilpivirine; ART=antiretroviral therapy.

* Number of RPV resistance-associated mutations among different HIV-1 subtypes.

† The detection rate of RPV resistance associated mutations among different HIV-1 subtypes.

Preplanned Studies

Identification and Genomic Characterization of *Corynebacterium belfantii* Strains — Fujian Province, China, 2019–2025

Wenwei Wu[1]; Yuhang Deng[1]; Rui Jin[1]; Junjie Mao[1]; Yadong Gao[2,3]; Quwen Li[1,2,3,#]

Summary

What is already known about this topic?

This is the first report of *Corynebacterium belfantii* (*C. belfantii*) in Fujian; genomic characterization confirms misidentification by routine methods and reveals regional phylogenetic characteristics.

What is added by this report?

This report adds the first local occurrence evidence, new genomic sequences, a distinct phylogenetic sub-branch, and a reinforced surveillance strategy for Fujian Province.

What are the implications for public health practice?

It emphasizes that laboratories should adopt molecular methods to accurately distinguish *C. belfantii*, strengthen surveillance of non-toxigenic strains, update MALDI-TOF databases, and monitor virulence and resistance genes despite the absence of diphtheria toxin.

ABSTRACT

Introduction: This study aimed to identify three non-toxigenic *Corynebacterium diphtheriae* (*C. diphtheriae*) complex strains isolated in Fujian Province between 2019 and 2025 and to determine their taxonomic classification through integrated phenotypic and genomic analyses.

Methods: Biochemical identification, matrix-assisted laser desorption/ionization time-of-flight mass spectrometry (MALDI-TOF MS), and polymerase chain reaction (PCR) were performed on three suspected *C. diphtheriae* isolates. Whole-genome sequencing was conducted using a nanopore sequencing platform. Average nucleotide identity (ANI) was calculated, and phylogenetic trees based on the 16S rRNA, the dtxR gene, and the pangenome were constructed, followed by comparative analysis against global NCBI sequences.

Results: All three strains were identified as *C. diphtheriae* by biochemical and mass spectrometric methods, with PCR detecting no tox gene carriage. ANI analysis showed 99.16%–99.22% identity with the reference genome GCA_041898185. This confirmed their classification as *C. belfantii*. Phylogenetic analysis indicated high conservation of the *dtxR* gene in *C. belfantii*. Pangenomic evolutionary trees showed that the Fujian strains clustered within the same major branch as global strains but formed a distinct sub-branch.

Conclusion: This study reports the first identification of *C. belfantii* in Fujian Province and describes its genomic characteristics and evolutionary position. These findings suggest that clinical and public health laboratories should use molecular methods to accurately distinguish members of the non-toxigenic *C. diphtheriae* complex and strengthen laboratory surveillance capacity.

Over 160 species of the genus *Corynebacterium* have been identified to date, among which *Corynebacterium diphtheriae* (*C. diphtheriae*), *Corynebacerium ulcerans* (*C. ulcerans*), and *Corynebacerium pseudotuberculosis* (*C. pseudotuberculosis)* are recognized as pathogenic species capable of producing diphtheria toxin (DT). Subsequently, the *C. diphtheriae* complex was formally defined, encompassing additional potentially toxigenic species, namely, *C. belfantii*, *C. rouxii*, and *C. silvaticum* (*1–2*). These key pathogens have substantial implications for global public health, with broad host ranges encompassing both humans, including *C. diphtheriae*, *C. belfantii*, and *C. rouxii,* and wild and domestic mammals, including *C. ulcerans*, *C. pseudotuberculosis*, and *C. silvaticum* (*1–2*). With advances in genomic identification technologies and molecular phylogenetic analysis methods, the understanding of the ecological and host niches and pathogenic factors of *Corynebacterium* species previously regarded as commensals, particularly those isolated from human samples, has progressively deepened, highlighting their clinical importance.

This study analyzed three non-toxigenic *C. diphtheriae* isolates obtained in Fujian Province from 2019–2025 through biochemical identification, mass spectrometry, polymerase chain reaction (PCR), and whole-genome sequencing. Comparative phylogenetic analysis with global National Center for Biotechnology Information (NCBI) sequences was performed to enhance epidemiological data on *Corynebacterium belfantii* and provide scientific evidence for public health laboratory diagnostics.

Three isolates, namely, FJ_201901, FJ_202501, and FJ_202502, from cases in Fujian Province were initially identified as *C. diphtheriae* by mass spectrometry and biochemical testing. Specimens were collected from the sputum, nasal secretions, and bronchoalveolar lavage fluid of female patients aged 25, 68, and 52 years, respectively. For comparative analysis, 33 *C. belfantii*, 15 *C. silvaticum*, six *C. rouxii*, three *C. diphtheriae* (strains NCTC11397, PW8, NCTC 13129), one *C. diphtheriae* bv. gravis (strain 5521/17), one *C. diphtheriae* bv. mitis (strain 230/19), and one *C. ulcerans* genome sequences were downloaded from NCBI, totaling 63 strains for analysis.

Preliminary identification was performed using matrix-assisted laser desorption/ionization time-of-flight mass spectrometry (MALDI-TOF MS), alongside biochemical identification using the VITEK CBC *Corynebacterium* identification card (bioMérieux China Ltd.). Strain identification was conducted using a *C. diphtheriae* nucleic acid detection kit (Shenzhen Bioyuan Life Science Co., Ltd.). Meanwhile, detection of the virulence gene *tox* in *C. diphtheriae* was performed using a duplex nucleic acid detection kit for *toxA* and *toxB* (Beijing Zhucheng Huisheng Biotechnology Co., Ltd.).

Genomic DNA was extracted using the DNeasy UltraClean Microbial Kit (QIAGEN, Venlo, The Netherlands). Library preparation was performed using the Rapid Genome Barcoding Kit (set)-24 (V3.0, Qitan Technology Co., Ltd., Chengdu), and sequencing was performed on the QNome-3841 platform (Qitan Technology Co., Ltd., Chengdu) using QDS (V3.0, Qitan Technology Co., Ltd., Chengdu) sequencing reagents. Following quality control using FastQC (version 0.12.1, Babraham Bioinformatics, Cambridge, UK), genomes were assembled using SPAdes (version 4.0.0, Saint Petersburg State University, St. Petersburg, Russia). Average nucleotide identity (ANI) was calculated using fastANI (version 1.34, GitHub, San Francisco, CA, USA). Single-nucleotide polymorphism (SNP) phylogenetic analysis was performed using snippy (version 4.6.0, Victorian Bioinformatics Consortium, Melbourne, Australia) for whole-genome alignment, followed by recombination removal using Gubbins (version 2.3.4, University of Oxford, Oxford, UK). FastTree (version 2.1.10, University of Washington, Seattle, WA, USA) was used for phylogenetic tree construction, with visualization in ChiPlot. Pangenome analysis was performed using Roary based on GFF3 files generated by Prokka(version 1.14.6, Victorian Bioinformatics Consortium, Melbourne, Australia).

All three strains yielded biochemical identification codes of 35431300405010, with a 95% probability of identification as *C. diphtheriae*. Mass spectrometry scores ranged from 2.25 to 2.31, indicating reliable identification as *C. diphtheriae*. Fluorescence PCR confirmed the absence of *toxA* and *toxB* genes in all three strains.

ANI analysis showed that Fujian strains FJ_201901, FJ_202501, and FJ_202502 shared 99.17%, 99.16%, and 99.22% identity, respectively, with the reference genome GCA_041898185. ANI values ranged from 94.85 to 100% compared with those of 33 other *C. belfantii strains*; from 79.28 to 79.94% with *C. silvaticum*; from 91.51 to 91.80% with *C. rouxii*; from 94.85 to 95.18% with *C. diphtheriae*; and from 79.61 to 79.82% with *C. ulcerans* (Figure 1). These results confirmed that FJ_201901, FJ_202501, and FJ_202502 were *C. belfantii*.

16S rRNA phylogenetic analysis indicated high conservation of the 16S rRNA gene throughout the genus *Corynebacterium*, establishing it as a reliable marker for genus-level classification (Figure 2). The clustering pattern resembled that of the *dtxR* gene tree (Figure 3), with strains clustering primarily by species or biovar. However, 16S rRNA could not distinguish extremely closely related strains or biovars, such as different virulence subtypes of *C. diphtheriae*. Meanwhile, the *dtxR* gene tree showed higher resolution. *C. belfantii* strains constituted the largest group, forming the main branch with relatively short branch lengths. This indicated high conservation of *dtxR* gene sequences within this species. Different biovars of *C. diphtheriae* (bv. *gravis*, bv. *mitis*) and related species (*C. ulcerans*, *C. silvaticum*, *C. rouxii*) formed independent small branches in the upper portion of the tree, consistent with their taxonomic positions. Independent clustering of *C. diphtheriae* biovars suggested that *dtxR* gene sequence

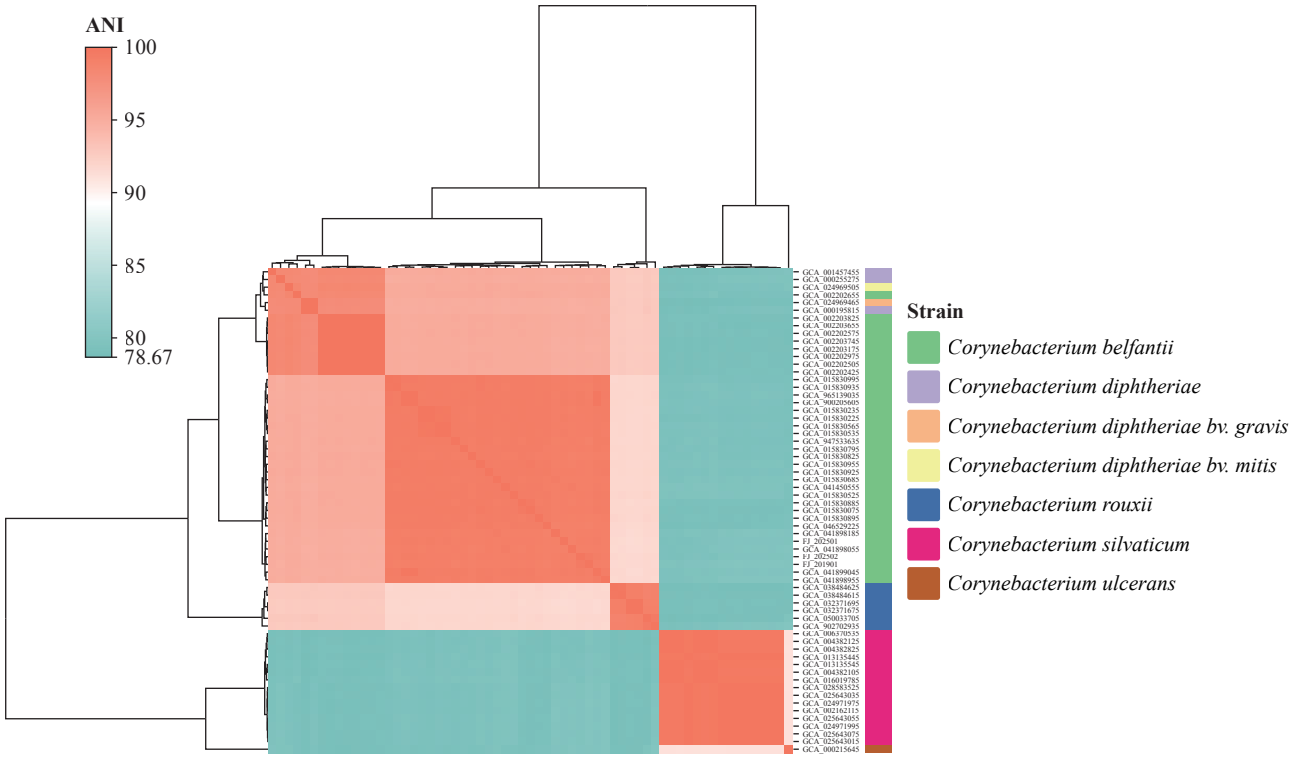

FIGURE 1. ANI analysis of 63 strains of the *Corynebacterium diphtheriae* complex.
Abbreviation: ANI=average nucleotide identity.

differentiation may correlate with virulence subtype evolution. This phylogenetic tree validated species differentiation patterns within *Corynebacterium* and provided molecular evolutionary evidence for subsequent investigation of associations between *dtxR* gene variation and virulence phenotypes. 16S rRNA phylogeny primarily serves to verify genus- and species-level taxonomic status, whereas *dtxR* gene phylogeny proves more suitable for exploring fine-scale evolutionary relationships within species, such as among different virulence subtypes.

To analyze genome evolution, virulence gene distribution, and the epidemiological characteristics of *Corynebacterium* strains, a phylogenetic tree was constructed based on Roary pangenome analysis. This analysis integrated multilocus sequence typing (MLST) and presence/absence information for key virulence genes (*narK*, *dtxR*, tox) (Figure 4). The tree scale (0.3) reflects genetic distances at the pangenome level, indicating substantial whole-genome differences among strains. The results showed clear clustering of all strains primarily by species or biovar, with *C. belfantii* constituting the largest group and exhibiting branch structures highly consistent with traditional taxonomy. Strains within certain branches shared geographic origins, such as China or France, or host types, such as human or swine, suggesting geographic or host specificity in strain transmission. The gene distribution matrix analysis indicated the conserved presence of *dtxR* across most strains. This finding is consistent with its role as a core regulatory gene, whereas *tox* genes were carried only by a few virulent *C. diphtheriae* biovars (bv. *gravis* and bv. *mitis*), correlating with pathogenic phenotypes. Carriage rates of other genes, such as *narK*, showed species specificity and may serve as auxiliary typing markers. Based on species annotation, non-pathogenic species, such as *C. belfantii*, generally lacked *tox* genes. Meanwhile, virulent biovars stably carried these genes, supporting the correlation between gene carriage and phenotype. The high resolution of the pangenome phylogenetic tree revealed fine-scale intra- and interspecies evolutionary relationships and provided whole-genome evidence. These findings, together with geographic and host information, provide a basis for tracing strain origins, transmission pathways, and cross-species transmission risks.

DISCUSSION

The *Corynebacterium diphtheriae* complex has undergone frequent taxonomic updates in recent years,

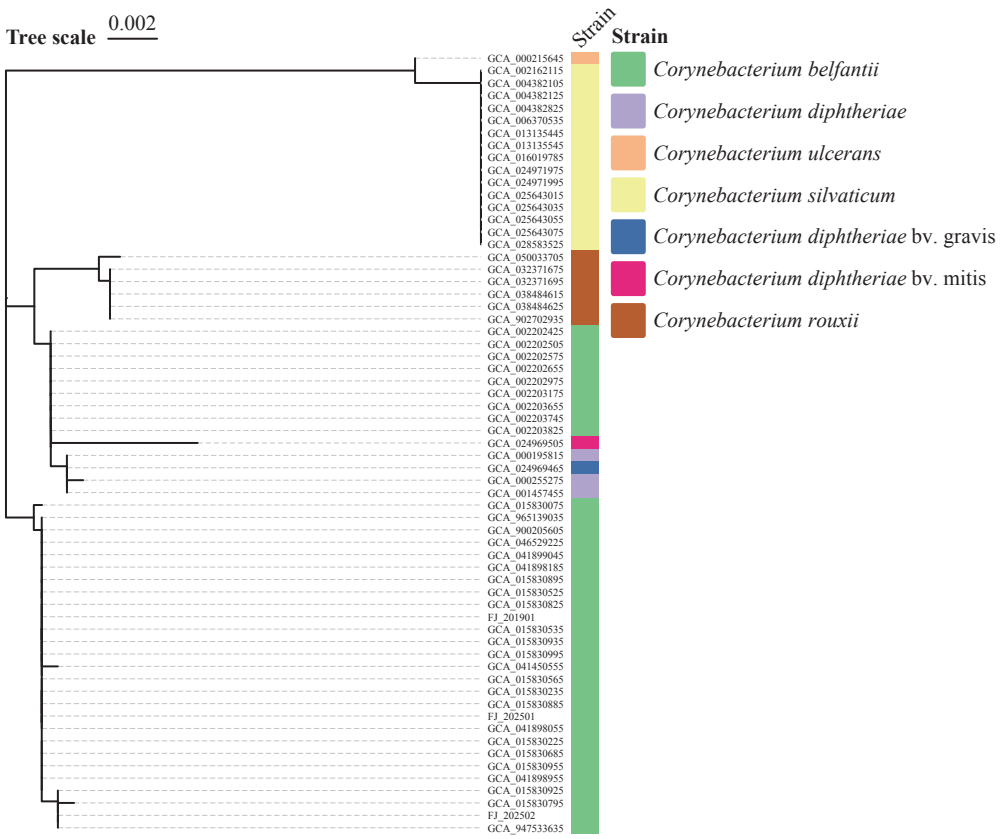

FIGURE 2. 16S rRNA gene-based phylogenetic tree of the *Corynebacterium diphtheriae* complex.
Abbreviation: rRNA=ribosomal RNA; RNA=ribonucleic acid.

with *C. belfantii*, a newly described species sharing high phenotypic similarity with classical *C. diphtheriae* but typically lacking *tox* gene carriage (*3*–*4*). This presents challenges for routine microbiological identification and epidemiological surveillance. To our knowledge, this study represents the first biochemical, mass spectrometric, molecular, and genomic analysis of three non-toxigenic *C. diphtheriae* strains isolated in Fujian Province between 2019 and 2025, confirming their classification as *C. belfantii*. Comparative phylogenetic analysis with global sequences preliminarily characterized their molecular characteristics, virulence regulatory mechanisms, and evolutionary status.

Traditional biochemical identification methods could not accurately identify the three strains as *C. belfantii* because of their highly similar biochemical metabolic profiles to those of *C. diphtheriae*. This highlights the limitations of phenotype-based identification systems in distinguishing closely related species within the complex. MALDI-TOF mass spectrometry similarly could not differentiate *C. belfantii* from closely related species within the complex because of the absence of *C. belfantii* in reference databases, highlighting the need for database updates or custom library construction for accurate identification. Through PCR, genome sequencing, and ANI analysis, the species classification of the three strains was definitively determined. This highlights the need for clinical and public health laboratories to establish molecular biology- or genomics-based confirmatory protocols as the gold standard for non-toxigenic *C. diphtheriae* isolates to prevent underdetection or misreporting.

Genomic analysis showed that all three *C. belfantii* strains lacked the *tox* gene cassette and lysogenic phage elements carrying this gene, consistent with the typically non-toxigenic nature of this species. Although *C. belfantii* does not produce diphtheria toxin, it retains the capacity for colonization and localized infection. Its public health relevance as an opportunistic pathogen should not be overlooked (*5*–*8*). The *dtxR* gene phylogenetic tree elucidated species clustering patterns and gene evolutionary characteristics within the genus *Corynebacterium*. The high conservation among *C. belfantii* strains in the

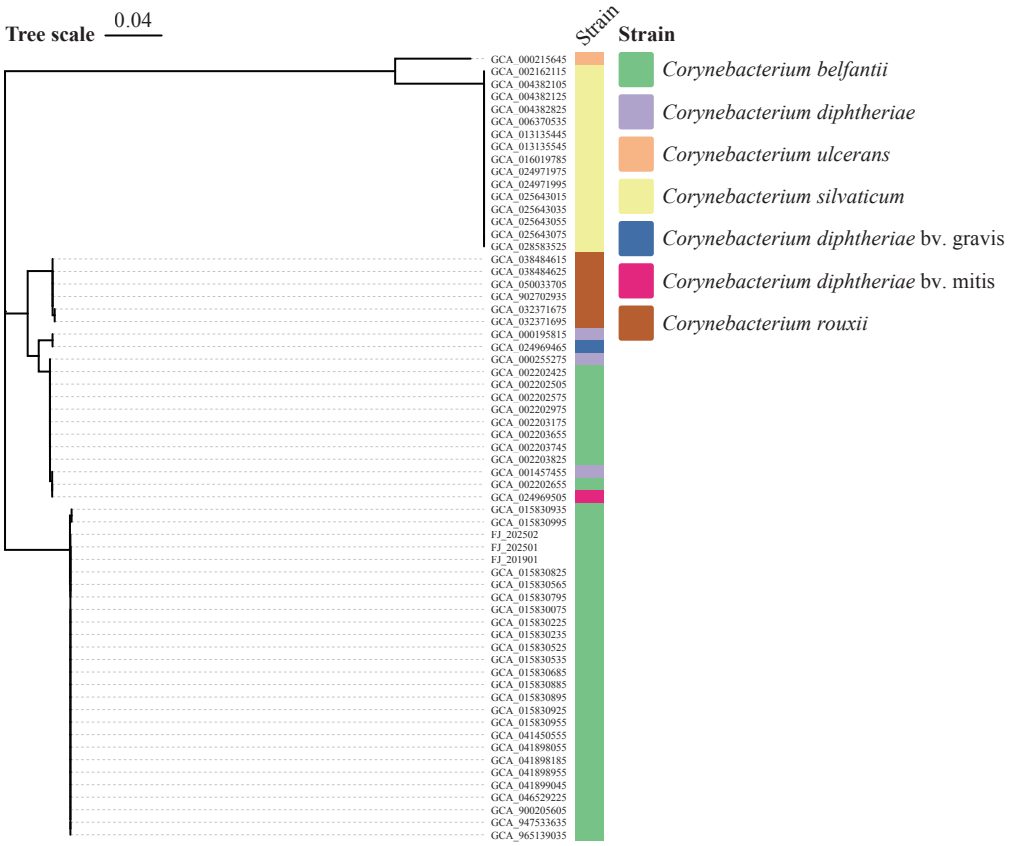

FIGURE 3. *dtxR* gene-based phylogenetic tree of the *Corynebacterium diphtheriae* complex..
Abbreviation: dtxR=diphtheria toxin repressor.

evolutionary tree suggests strong purifying selection pressure on the *dtxR* gene in this species. This is consistent with its non-pathogenic or weakly pathogenic phenotype. Independent clustering of different *C. diphtheriae* biovars (*gravis* and *mitis*) suggests that *dtxR* gene sequence variation may co-occur with virulence subtype differentiation. This finding aligns with previous reports associating diphtheria toxin expression levels with biovars, supporting the central role of *dtxR* in virulence regulation (*9–12*). Branching relationships among closely related species *C. ulcerans*, *C. silvaticum*, and *C. diphtheriae* reflect the balance between conservation and variation of the *dtxR* gene during species evolution. This validates the taxonomic framework of *Corynebacterium* and provides molecular evidence for tracing the horizontal transfer and evolutionary pathways of virulence genes.

Further pangenome-based phylogenetic tree construction, combined with MLST typing and virulence gene analysis, revealed evolutionary patterns and virulence characteristics of *Corynebacterium* at the whole-genome level. The high resolution of the pangenome phylogenetic tree revealed genomic differences among strains, with clustering patterns highly consistent with traditional taxonomy. This supports the reliability of the species classification. Whole-genome SNP-based phylogenetic trees showed that the three Fujian *C. belfantii* strains (FJ_201901, FJ_202501, and FJ_202502) clustered within the same major branch as strains from the NCBI database (GCA_015830685, GCA_041450555, GCA_041898055, GCA_041898955, and GCA_041898185), indicating close genetic relationships. Strain FJ_201901 and FJ_202501 clustered in the same sub-branch, suggesting a possible cross-regional transmission or a shared evolutionary origin. However, the Fujian strains also formed an independent small cluster, implying potential regional microevolutionary characteristics.

The conserved presence of the virulence regulatory gene *dtxR* across all 63 strains indicates its fundamental function as a core regulatory gene in this bacterial genus. Meanwhile, *tox* gene carriage exclusively in a few virulent *C. diphtheriae* biovars suggests that acquisition of diphtheria toxin represents a critical

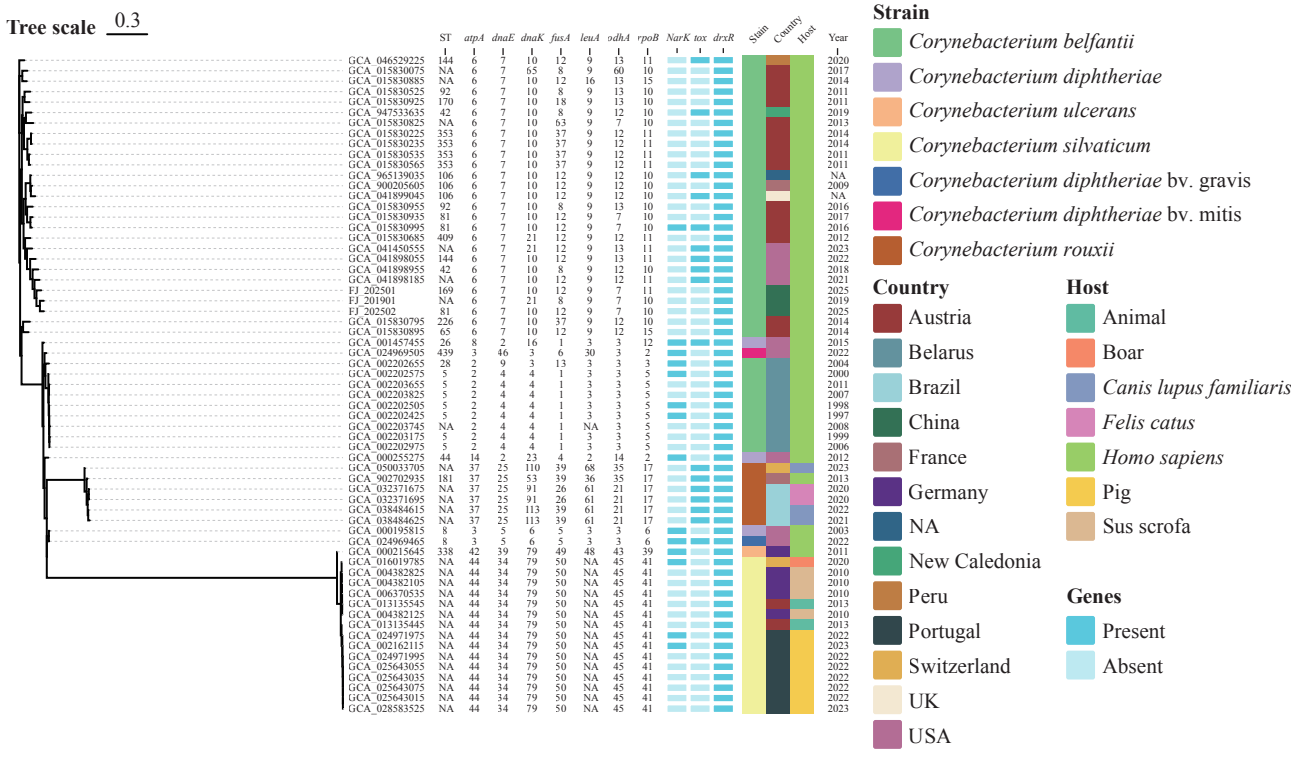

FIGURE 4. Roary-based core-genome phylogenetic tree of the *Corynebacterium diphtheriae* complex.
Abbreviation: MLST=multilocus sequence typing; narK=nitrate reductase; dtxR=diphtheria toxin repressor; tox=diphtheria toxin; NA=Not applicable; UK=United Kindom; USA=United States of America.

event in the evolution of high pathogenicity, with stable inheritance restricted to specific lineages. This distribution pattern aligns with clinical observations that diphtheria cases are caused only by specific virulent strains. This also provides molecular targets for the rapid screening of virulent strains. Comparison of the pangenome analysis with single-gene phylogenetic trees, such as 16S rRNA and *dtxR* phylogenetic trees, showed that pangenome phylogeny enables higher-resolution analysis of intraspecies and interbiovar evolutionary relationships. Combined with the MLST typing results, this facilitates tracing of strain origins and transmission pathways, providing robust supporting data for tracking strain sources and understanding global dissemination patterns. Future studies should incorporate additional Asian strain sequences for comparison to more clearly delineate regional epidemiological characteristics of *C. belfantii*.

The findings of this study have implications for laboratory surveillance of diphtheria and diphtheria-like diseases. First, the carriage rate of non-toxigenic *C. diphtheriae* complex strains in human populations may be underestimated, particularly under immune pressure, where these strains might fill ecological niches. Second, laboratories should enhance identification capabilities by avoiding the misidentification of *C. belfantii* as non-toxigenic *C. diphtheriae* and instead using accurate species names to accumulate precise epidemiological data. Third, the conservation of *dtxR* as a core virulence regulatory element suggests its potential as a molecular detection target for assessing strain virulence potential. Although *C. belfantii* does not produce diphtheria toxin, carriage of other virulence and resistance genes warrants continued monitoring.

However, this study has certain limitations. First, the small sample size, that is, only three strains from specific regions and time periods, may not fully reflect the prevalence patterns and genetic diversity of *C. belfantii* in Fujian Province or throughout China. Second, the lack of detailed clinical data, such as patient symptoms, vaccination history, and underlying diseases, limits the assessment of the actual pathogenic risk and clinical relevance of these strains. Future studies should expand the sample size, conduct case-control studies incorporating clinical data, and perform in vitro cellular and in vivo animal model validation of pathogenic potential. Genome-wide association studies (GWAS) should be used to further elucidate associations between genomic variations and virulence

phenotypes or host adaptation, particularly the impact of *dtxR* gene variants on strain virulence phenotypes. This can provide more precise molecular targets for diphtheria and related disease prevention and control.

Conflicts of interest: No conflicts of interest.

Funding: Supported in part by a grant from the Fujian Provincial Science and Technology Plan Project (2026J0011260).

doi: 10.46234/ccdcw2026.148

[#] Corresponding author: Quwen Li, lqw0043@163.com.

[1] School of Public Health, Fujian Medical University, Fuzhou City, Fujian Province, China; [2] Fujian Provincial Center for Disease Control and Prevention, Fuzhou City, Fujian Province, China; [3] Fujian Provincial Key Laboratory of Zoonoses Research, Fujian Provincial Institute of Preventive Medicine, Fuzhou City, Fujian Province, China.

Submitted: May 09, 2026
Accepted: June 26, 2026
Issued: July 17, 2026

REFERENCES

1. Mitchell BI, Markantonis JE. An underestimated pathogen: *Corynebacterium* species. J Clin Microbiol 2025;63(10):e01552 – 24. https://doi.org/10.1128/jcm.01552-24.
2. Dazas M, Badell E, Carmi-Leroy A, Criscuolo A, Brisse S. Taxonomic status of *Corynebacterium diphtheriae* biovar Belfanti and proposal of *Corynebacterium belfantii* sp. nov. Int J Syst Evol Microbiol 2018;68 (12):3826 – 31. https://doi.org/10.1099/ijsem.0.003069.
3. Peng YH, Fueston H, Irfan M, Hammond J, Morales D, Ju H, et al. Complete genome sequences of four representative *Corynebacterium belfantii* strains. Microbiol Resour Announc 2024;13(11):e00755 – 24. https://doi.org/10.1128/MRA.00755-24.
4. Pivot D, Fanton A, Badell-Ocando E, Benouachkou M, Astruc K, Huet F, et al. Carriage of a single strain of nontoxigenic *Corynebacterium diphtheriae* bv. Belfanti (Corynebacterium belfantii) in four patients with cystic fibrosis. J Clin Microbiol 2019;57(5):e00042 – 19. https://doi.org/10.1128/JCM.00042-19.
5. Burkovski A. Proteomics of toxigenic corynebacteria. Proteomes 2024;12(1):2. https://doi.org/10.3390/PROTEOMES12010002.
6. Ramos JN, Araújo MRB, Baio PVP, Sant'Anna LO, Veras JFC, Vieira ÉMD, et al. Molecular characterization and phylogenetic analysis of the first *Corynebacterium rouxii* strains isolated in Brazil: a recent member of *Corynebacterium diphtheriae* complex. BMC Genom Data 2023;24(1): 65. https://doi.org/10.1186/S12863-023-01167-W.
7. Viana MVC, Profeta R, Cerqueira JC, Vattam AR, Barh D, Silva A, et al. Evidence of episodic positive selection in *Corynebacterium diphtheriae* complex of species and its implementations in identification of drug and vaccine targets. PeerJ 2022;10:e12662. https://doi.org/10.7717/PEERJ.12662.
8. Hoefer A, Pampaka D, Herrera-León S, Peiró S, Varona S, López-Perea N, et al. Molecular and epidemiological characterization of toxigenic and nontoxigenic *Corynebacterium diphtheriae, Corynebacterium belfantii, Corynebacterium rouxii*, and *Corynebacterium ulcerans* isolates identified in Spain from 2014 to 2019. J Clin Microbiol 2021;59(3): e02410 – 20. https://doi.org/10.1128/JCM.02410-20.
9. Li QW, Liang XC, Gao YD, Weng ST, Gao Y, Shao ZJ. Epidemiological and pathogenic analyses of three cases of imported *Corynebacterium diphtheriae* infection in Fujian Province. Chin J Zoonoses 2024;40(6):590 – 4,598. https://doi.org/10.3969/j.issn.1002-2694.2024.00.081.
10. Li ZC, Liu MZ, Fang YM, Gong ZJ, Wang XL, Chen JD, et al. Identification and analysis of 2 Corynebacterium diphtheria strains in Guangdong Province. Chin J Prev Med 2022;56(4):427 – 32. https://doi.org/10.3760/cma.j.cn112150-20210517-00478.
11. Lyman LR, Peng ED, Schmitt MP. DtxR is a global iron-dependent regulatory protein with multiple roles in the control of gene expression in *Corynebacterium diphtheriae*. J Bacteriol 2026;208(3):e00530 – 25. https://doi.org/10.1128/JB.00530-25.
12. Valenzuela-Cardenas MB, Goodfellow SM. Microbe snapshot: corynebacterium diphtheriae. Clin Microbiol Newsl 2026;54:1 – 3. https://doi.org/10.1016/J.CLINMICNEWS.2025.11.001.

Outbreak Reports

First Human Infection with Influenza A(H1N2)v Virus — Yunnan Province, China, 2026

Lihua Chen[1,2]; Yaoyao Chen[3]; Xiaoyu Han[3]; Ruize Ni[3]; Ming Zeng[4]; Jie Deng[4]; Chunyuan Deng[5]; Guijing Chen[5]; Xiaoqing Fu[3]; Jibo He[1]; Chunrui Luo[3,#]

Summary

What is already known about this topic?

Human infections with influenza A(H1N2)v viruses of swine origin have been sporadically reported in several countries, usually following direct or indirect exposure to pigs or contaminated environments. However, sustained human-to-human transmission has not yet been documented.

What is added by this report?

This report describes the first laboratory-confirmed human infection with the influenza A(H1N2)v virus in China. Whole-genome sequencing showed that all eight gene segments were closely related to influenza viruses of swine origin circulating in China. No secondary human cases were identified among the close contacts, and no evidence of sustained human-to-human transmission was detected.

What are the implications for public health practice?

This highlights the importance of routine influenza-like illness surveillance, timely whole-genome sequencing, and systematic investigation of unusual influenza A infections. Strengthened surveillance at the human-animal interface and cross-sector collaboration under the One Health framework are essential for early detection and risk assessment of variant influenza viruses.

ABSTRACT

Introduction: Human infections with swine-origin influenza A(H1N2)v viruses have been reported sporadically worldwide, usually following direct or indirect exposure to pigs or contaminated environments. This report describes the first laboratory-confirmed human infection with influenza A(H1N2)v virus in China.

Methods: Following detection of a human infection with influenza A(H1N2)v virus through influenza-like illness surveillance in Yunnan Province in January 2026, an epidemiological investigation, close-contact tracing, animal and environmental sampling, and laboratory testing were conducted. Throat swab specimens were collected for real-time RT-PCR and whole-genome sequencing. Representative influenza virus sequences from the GISAID database were used for sequence comparison and phylogenetic analysis.

Results: A 2-year-old boy presented with fever, cough, and rhinorrhea, and recovered after antiviral, antibacterial, and supportive treatments. Whole-genome sequencing revealed the full-length sequences of all eight gene segments. The virus shared the highest nucleotide homology with swine-origin influenza viruses circulating in China, with nucleotide identities ranging from 95.17% to 98.53%, suggesting a reassortant swine-origin influenza A(H1N2)v virus. Epidemiological investigations revealed no clear history of direct contact with pigs or poultry, although the pigs and poultry were raised near the patient's residence. A total of 47 environmental samples and 28 animal samples were collected during the field investigation. Low viral loads of influenza A virus were detected in some swine and environmental samples; however, full subtyping and sequencing could not be performed for some samples because of low viral loads. Thirty close contacts were traced, and none developed relevant symptoms. No secondary cases or evidence of sustained human-to-human transmission was identified.

Conclusion: This case suggests a sporadic zoonotic transmission event with limited public health risk.

Variant influenza viruses originating from swine represent an ongoing threat to global public health, owing to their genetic diversity and capacity for reassortment (*1*). When swine influenza viruses infect humans, they are designated with the suffix "v" according to World Health Organization (WHO)

nomenclature. According to WHO influenza nomenclature, the suffix "v" is placed outside the subtype parentheses; therefore, the virus described in this report is referred to as influenza A(H1N2)v virus, rather than influenza A(H1N2)v virus. Although most variant influenza infections result in mild illness and limited human-to-human transmission, sporadic zoonotic events underscore the importance of integrated surveillance under the One Health framework (*2*).

Influenza A(H1N2)v virus has been sporadically reported in several countries and is primarily associated with direct or indirect exposure to pigs. To date, sustained human-to-human transmission has not been documented. In China, swine influenza A(H1N2) viruses have been detected in pig populations, and previous genetic studies have shown that swine influenza viruses circulating in China are genetically diverse and may undergo reassortment among H1N1, H1N2, H3N2, and other swine-origin influenza virus lineages. These findings indicate that swine influenza A virus circulating in domestic pig populations may pose a zoonotic risk. Human infections with A(H1N2)v are rare, and no confirmed cases have been reported in China prior to this event (*3*). Here, we report the first laboratory-confirmed human infection with A(H1N2)v virus detected through influenza-like illness (ILI) sentinel surveillance in Yunnan Province and describe the comprehensive field investigation and response measures undertaken (*4*). This case has public health significance because it represents the first recognized human A(H1N2)v infection in China and highlights the value of routine influenza surveillance for detecting rare variant influenza virus infections.

METHODS

Case Detection

On January 30, 2026, the Provincial CDC identified influenza A(H1N2)v virus in a respiratory specimen collected from an ILI patient at a sentinel hospital. The specimen was collected on January 26, 2026, at a local children's hospital, and the clinical specimen used for case confirmation was a throat swab. Initial screening for influenza A virus and subtype confirmation were conducted by the local CDC.

Case Definition

A suspected human infection with a variant influenza virus was defined as an acute respiratory illness with laboratory evidence of influenza A virus infection that could not be subtyped as currently circulating seasonal influenza viruses or that showed subtype characteristics suggestive of swine-origin influenza virus infection. A confirmed case was defined as a respiratory specimen positive for influenza A virus and laboratory evidence of swine-origin influenza A(H1N2)v infection by subtype-specific real-time RT-PCR and/or whole-genome sequencing (*5*).

Field Investigation

Upon confirmation, the local CDC dispatched a multidisciplinary investigation team comprising epidemiologists, laboratory specialists, and emergency response personnel to conduct field investigations, including case interviews, contact tracing, environmental assessments, and animal sampling.

We collected information on the patient's clinical course, healthcare-seeking history, travel history, animal exposure history, household environment, and contact history during the 10 days prior to illness onset.

Close Contact Definition and Management

Close contacts were defined as persons who had unprotected close contact with the patient from one day before illness onset to discharge, including household members, caregivers, healthcare workers, and other persons with close exposure in enclosed settings. All close contacts were placed under medical observation for seven days after their last exposure. Respiratory specimens were collected from close contacts during the investigation and tested using real-time RT-PCR. The investigators also asked whether close contacts developed an influenza-like illness before the onset of the patient's illness.

Laboratory Testing

Respiratory specimens were tested using real-time RT-PCR for influenza A virus and subtyped for the H and N genes. Real-time RT-PCR was performed using a Rapid Typing Kit for Influenza A Virus HxNy. The primers and probes used for H and N gene subtyping are included in the kit. Testing was conducted according to the manufacturer's instructions. Whole-genome sequencing was performed using next-generation sequencing (NGS). In the present study,

sequencing was performed using the MiniSeq next-generation sequencing system. The sequencing data were analyzed using CLC Genomics Workbench (version 23.0; QIAGEN, Aarhus, Denmark). Sequence assembly and analysis revealed the full-length sequences of all eight gene segments. Alignment with the GISAID database indicated that all gene segments shared the highest sequence homology with swine-origin influenza viruses prevalent in China, identifying the virus as a swine-origin influenza A (H1N2)v virus.

Phylogenetic analysis was conducted by comparing the human viral sequences obtained with representative domestic and international influenza virus sequences available from Global Initiative on Sharing All Influenza Data (GISAID). Full-length sequences of all eight gene segments were obtained from human cases, and phylogenetic trees were constructed to clarify the genetic origin of each segment. However, full viral genome sequences could not be obtained from influenza A-positive animals and environmental samples because of low viral loads; therefore, accession numbers for these samples were not available. The nucleotide sequences generated from the human case were not submitted to GISAID or GenBank; therefore, no accession numbers were available, and virus isolation was unsuccessful because of low viral load and/or insufficient viable virus in the residual specimens.

Animal and Environmental Sampling

A total of 47 environmental and 28 animal specimens were collected during the field investigation. Animal and environmental specimens included pig nasopharyngeal swabs, poultry oropharyngeal and cloacal swabs, fecal samples, feed and drinking water samples, environmental surface swabs, wastewater samples, and tissue or fluid specimens from a dead pig in a neighboring household. All specimens were screened for influenza A virus, and influenza A-positive specimens were further tested for the H5, H7, H9, and HxNy subtypes when the viral load was allowed.

Ethical Considerations

All the investigations were conducted as part of a public health emergency. Personal identifiers were anonymized to protect patient privacy. This investigation was conducted during routine infectious disease surveillance and public health emergency response activities.

RESULTS

Case Description

The patient was a 2-year-old boy residing in Yunnan Province. He lived in a rural household with his grandparents and other family members. His parents were migrant workers living outside the county.

The patient developed a fever with a maximum temperature of 38.9 °C, cough, and rhinorrhea on January 20, 2026, following cold exposure. He initially sought care at a township health center and later at a private clinic, which was a different healthcare facility from the township health center. He was treated with antipyretics, antibiotics, and antiviral medications without significant improvement. Owing to persistent fever, he was transferred to Kunming on January 25 and admitted to a local Children's Hospital on January 26. On admission, a physical examination revealed pharyngeal congestion, tonsillar enlargement, and coarse breath sounds with sputum rales. Laboratory tests showed elevated C-reactive protein levels but normal white blood cell counts. Respiratory pathogen testing was positive for influenza A virus. Chest radiography indicated increased bilateral lung markings. *Haemophilus influenzae* coinfection was diagnosed based on nucleic acid testing of a throat swab collected from the patient and performed by the hospital laboratory.

The patient was diagnosed with pneumonia complicated by influenza A virus and Haemophilus influenzae infections. The patient was treated with oseltamivir, cefoperazone–sulbactam, nebulized budesonide, and supportive therapy, resulting in clinical improvement. The patient was discharged on January 31, 2026 (Figure 1).

On January 20, 2026, the patient developed influenza-like symptoms and sought medical care multiple times before hospital admission on January 26. Laboratory confirmation of influenza A(H1N2)v was obtained on January 30, and the patient recovered and was discharged on January 31, 2026.

Epidemiological Investigation

The patient lived in a rural village, where pigs, chickens, and pigeons were raised. Family members denied direct contact between the patient and the livestock. The patient had no travel history or exposure to live poultry markets in the 10 days prior to

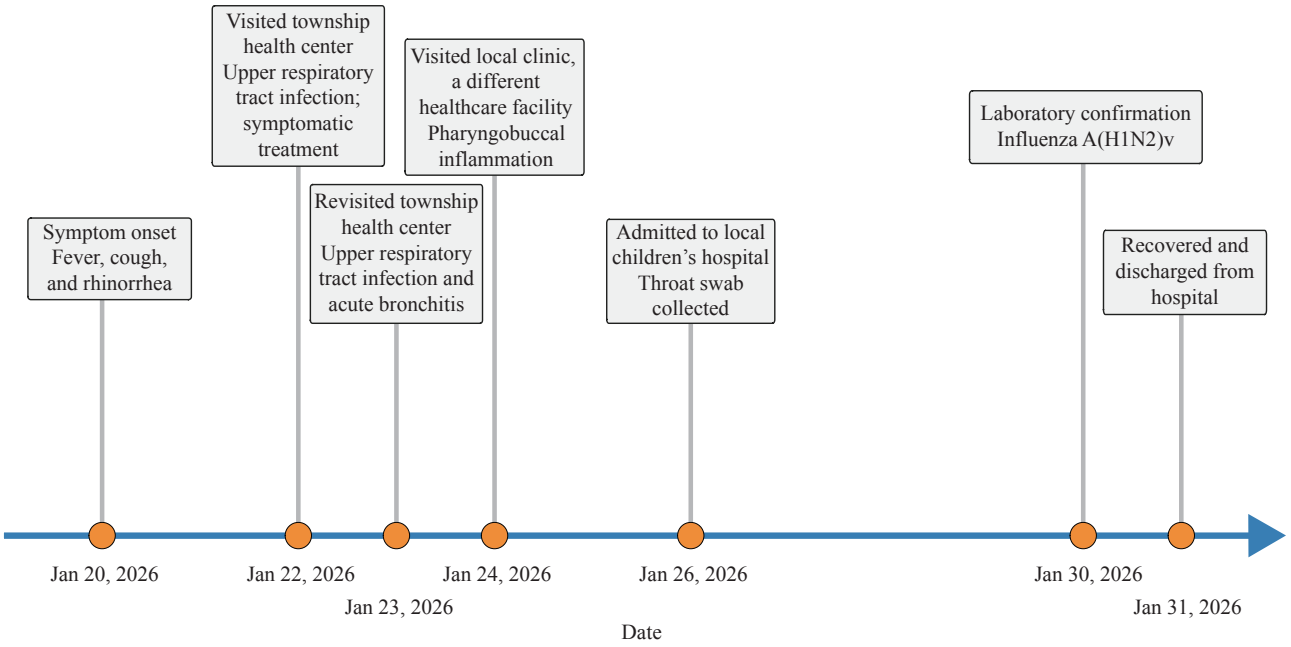

FIGURE 1. Timeline of symptom onset, healthcare visits, diagnosis, and recovery of the patient.

symptom onset. Although no direct animal contact was reported, the presence of pigs and poultry near the living area suggested the possibility of indirect environmental exposure.

A detailed activity history revealed that the patient remained primarily at home during the incubation period, with close contacts limited to household members who stayed mainly at home, used personal items such as a bed, feeding bottle, toys, and had contact mainly with grandparents, relatives, and occasional neighbors. No direct contact with poultry or livestock has been reported (Table 1).

Thirty close contacts including household members, healthcare workers, and caregivers were identified. All contacts were monitored for symptoms and tested using RT-PCR. No secondary cases were identified in this study.

Environmental and Animal Investigation

The patient's residence comprised stone and brick structures with suboptimal sanitation. Pig and poultry enclosures were adjacent to the living areas. Environmental hygiene was poor, with visible poultry feces in courtyards (Figure 2).

Multiple rounds of animal sampling were conducted on pigs, chickens, geese, pigeons, and environmental surfaces. Most specimens tested negative for the

TABLE 1. Activity and exposure history of the case during the 10 days prior to illness onset.

Date	Location	Items involved	Persons in contact	Contact with poultry or livestock
Jan-10-2026	Home	Bed, feeding bottle, toys	Grandfather, grandmother, neighbor	No direct contact
Jan-11-2026	Home	Bed, feeding bottle, toys	Grandmother, grandfather	No direct contact
Jan-12-2026	Home	Bed, feeding bottle, toys	Grandmother, grandfather, great-uncle	No direct contact
Jan-13-2026	Home	Bed, feeding bottle, toys	Grandmother, aunt, grandfather, uncle	No direct contact
Jan-14-2026	Home	Bed, feeding bottle, toys	Grandmother, aunt, grandfather, uncle, great-uncle	No direct contact
Jan-15-2026	Home	Bed, feeding bottle, toys	Grandmother, aunt, grandfather, uncle	No direct contact
Jan-16-2026	Home	Bed, feeding bottle, toys	Grandmother, aunt, grandfather, uncle	No direct contact
Jan-17-2026	Home	Bed, feeding bottle, toys	Grandmother, aunt, grandfather, uncle	No direct contact
Jan-18-2026	Home	Bed, feeding bottle, toys	Grandmother, aunt, grandfather, uncle	No direct contact
Jan-19-2026	Home	Bed, feeding bottle, toys	Grandmother, aunt, grandfather, uncle	No direct contact

Abbreviation: Jan=January.

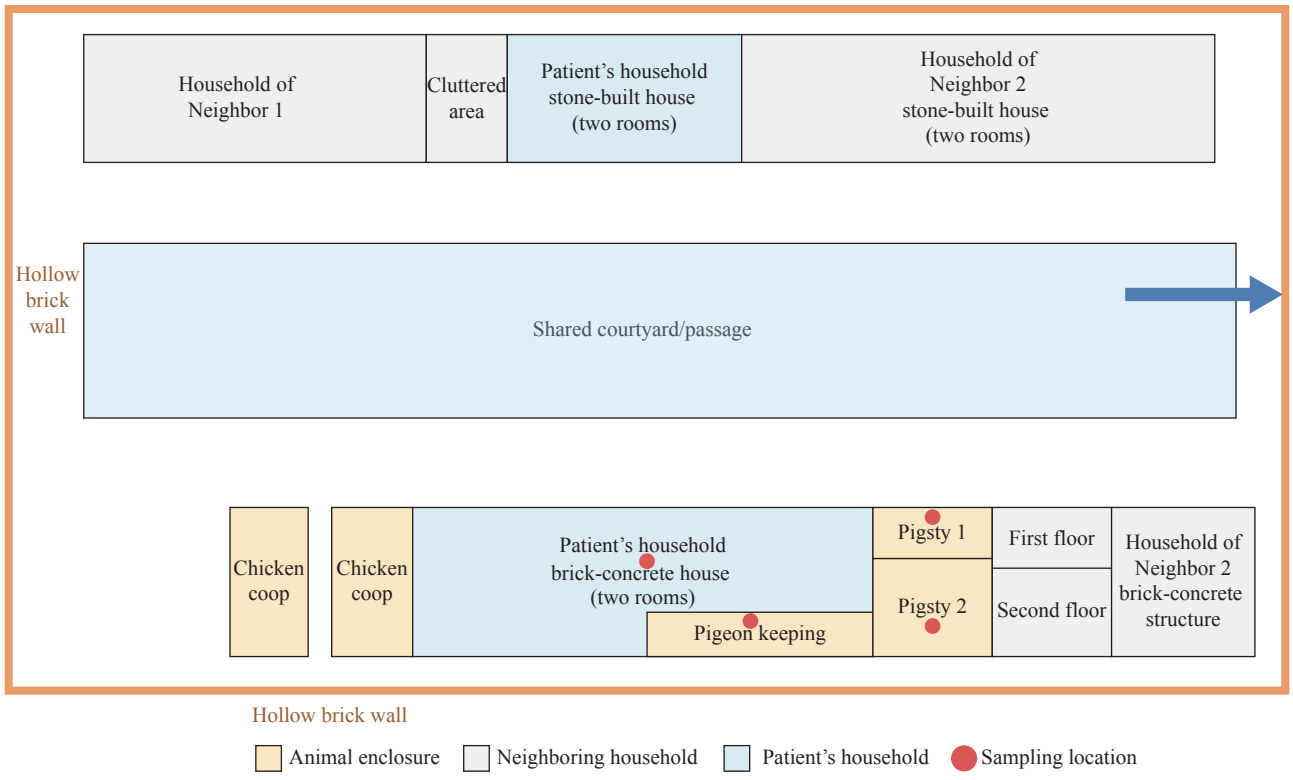

FIGURE 2. Layout of the patient's household and surrounding livestock facilities

influenza A virus. However, low loads of influenza A virus were detected in a small number of pig and environmental samples [cycle threshold (Ct) values >35] (Table 2).

Laboratory Findings

The patient's throat swab tested positive for influenza A virus (Ct 31.10), H1 subtype (Ct 27.41), and N2 subtype (Ct 26.68), confirming infection with influenza A(H1N2)v.

Whole-genome sequencing demonstrated that all eight gene segments clustered with influenza viruses of swine origin circulating in China, with nucleotide homology ranging from 95.17% to 98.53%. Internal genes originated from reassortment among swine H1N1, H1N2, and H3N2 viruses, and sequence assembly and analysis revealed the full-length sequences of all eight gene segments. Alignment with the GISAID database indicated that the virus shared the highest sequence homology with influenza viruses of swine origin prevalent in China, which identified the virus as a swine-origin influenza A(H1N2)v virus. Further whole-genome sequencing and sequence analysis conducted by China CDC confirmed that the specimen was positive for swine-origin influenza A(H1N2)v virus. According to the World Health Organization nomenclature, because an H1N2 swine influenza virus infected a human, the suffix "v" (variant) was added, and the virus was therefore designated influenza A(H1N2)v. Amino acid analysis showed that no known critical mutations were detected. Similar to previously identified H1 swine influenza viruses in China, the HA receptor-binding site at amino acid position 222 was E, suggesting dual receptor-binding characteristics. The HA cleavage site did not contain multiple basic amino acids, indicating that the virus was of low pathogenicity. The PB2 protein carried SR at positions 590–591, suggesting mammalian adaptation, while positions 627 and 701 remained E and D, respectively, with no mutation detected. No mutations associated with resistance to neuraminidase inhibitors or polymerase inhibitors were identified, suggesting sensitivity to these antiviral drugs.

Further investigation identified an N2-positive sample from the lung tissue of a pig that had died in a neighboring household. However, because the viral load of the positive animal specimen was low, and full viral sequencing could not be obtained from animal or environmental samples, direct genomic evidence

TABLE 2. Detection of influenza A virus in animal and environmental samples during field investigation.

Surveillance site	Sample ID / source	Specimen type	Collection date	Influenza A result	H5	H7	H9	HxNy subtyping
Patient's household	Pig 1	Nasopharyngeal swab	Jan-31-2026	Negative	Negative	Negative	Negative	Negative
Patient's household	Pig 2	Nasopharyngeal swab	Jan-31-2026	Positive, Ct=36.58*	Negative	Negative	Negative	Not subtyped due to low viral load
Patient's household	Pig 3	Nasopharyngeal swab	Jan-31-2026	Positive, Ct=37.45*	Negative	Negative	Negative	Not subtyped due to low viral load
Patient's household	Pig feces	Fecal sample	Jan-31-2026	Negative	Negative	Negative	Negative	Negative
Patient's household	Pig feed trough	Surface swab	Jan-31-2026	Negative	Negative	Negative	Negative	Negative
Patient's household	Chicken feces	Fecal sample	Jan-31-2026	Negative	Negative	Negative	Negative	Negative
Patient's household	Chicken feed	Feed sample	Jan-31-2026	Negative	Negative	Negative	Negative	Negative
Patient's household	Chicken drinking water	Poultry drinking water	Jan-31-2026	Negative	Negative	Negative	Negative	Negative
Patient's household	Chicken	Oropharyngeal and cloacal swab	Jan-31-2026	Negative	Negative	Negative	Negative	Negative
Patient's household	Goose	Oropharyngeal and cloacal swab	Jan-31-2026	Negative	Negative	Negative	Negative	Negative
Patient's household	Pigeon	Oropharyngeal swab	Jan-31-2026	Negative	Negative	Negative	Negative	Negative
Patient's household	Bed frame in bedroom	Surface swab	Jan-31-2026	Negative	Negative	Negative	Negative	Negative
Patient's household	Pillow in patient's bedroom	Surface swab	Jan-31-2026	Positive, Ct=38.61*	Negative	Negative	Negative	Not subtyped due to low viral load
Patient's household	Medicine bowl	Surface swab	Jan-31-2026	Negative	Negative	Negative	Negative	Negative
Patient's household	Quilt in patient's bedroom	Surface swab	Jan-31-2026	Positive, Ct=36.31*	Negative	Negative	Negative	Not subtyped due to low viral load
Patient's household	Child's toy car	Surface swab	Jan-31-2026	Positive, Ct=36.16*	Negative	Negative	Negative	Not subtyped due to low viral load
Patient's household	Pigeon cage	Surface swab	Jan-31-2026	Negative	Negative	Negative	Negative	Negative
Neighbor1s household	Pig 4	Nasopharyngeal swab	Jan-31-2026	Positive, Ct=38.72*	Negative	Negative	Negative	Not subtyped due to low viral load
Neighbor1s household	Pig 5	Nasopharyngeal swab	Jan-31-2026	Negative	Negative	Negative	Negative	Negative
Neighbor1s household	Pig 6	Nasopharyngeal swab	Jan-31-2026	Negative	Negative	Negative	Negative	Negative
Neighbor1s household	Pig 4 feces	Fecal sample	Jan-31-2026	Negative	Negative	Negative	Negative	Negative
Slaughterhouse	Chopping board	Surface swab	Jan-31-2026	Negative	Negative	Negative	Negative	Negative
Slaughterhouse	Wastewater	Cleaning wastewater	Jan-31-2026	Negative	Negative	Negative	Negative	Negative
Clinic	Heated table	Surface swab	Jan-31-2026	Negative	Negative	Negative	Negative	Negative
Hospital	Bedside cabinet	Environmental swab	Jan-30-2026	Negative	Negative	Negative	Negative	Negative
Hospital	Bed rail	Environmental swab	Jan-30-2026	Negative	Negative	Negative	Negative	Negative
Hospital	Mobile phone	Environmental swab	Jan-30-2026	Negative	Negative	Negative	Negative	Negative
Hospital	Bathroom door handle	Environmental swab	Jan-30-2026	Negative	Negative	Negative	Negative	Negative
Hospital	Toilet flush button	Environmental swab	Jan-30-2026	Negative	Negative	Negative	Negative	Negative

Continued

Surveillance site	Sample ID / source	Specimen type	Collection date	Influenza A result	H5	H7	H9	HxNy subtyping
Hospital	Patient pillow	Environmental swab	Jan-30-2026	Negative	Negative	Negative	Negative	Negative
Hospital	Nebulizer tubing	Environmental swab	Jan-30-2026	Negative	Negative	Negative	Negative	Negative
Hospital	Consultation room	Environmental swab	Jan-30-2026	Negative	Negative	Negative	Negative	Negative
Patient's household	Wastewater 1	Water sample	Feb-3-2026	Negative	Negative	Negative	Negative	Negative
Patient's household	Pig feeding trough	Surface swab	Feb-3-2026	Negative	Negative	Negative	Negative	Negative
Neighbor's household	Wastewater 2	Water sample	Feb-3-2026	Negative	Negative	Negative	Negative	Negative
Neighbor's household	Pig feeding trough 3	Surface swab	Feb-3-2026	Negative	Negative	Negative	Negative	Negative
Neighbor1's household	Bronchoalveolar fluid	BAL fluid	Feb-1-2026	Positive, Ct=37.16*	Negative	Negative	Negative	Not subtyped due to low viral load
Neighbor2's household	Pleural effusion 1	Pleural fluid	Feb-1-2026	Negative	Negative	Negative	Negative	Negative
Neighbor2's household	Pleural effusion 2	Pleural fluid	Feb-1-2026	Negative	Negative	Negative	Negative	Negative
Neighbor2's household	Lung tissue 1	Lung tissue	Feb-1-2026	Positive, Ct=35.43*	Negative	Negative	Negative	Hx not subtyped; N2 suspected, Ct=37.85*
Neighbor2's household	Trachea	Tracheal tissue	Feb-1-2026	Negative	Negative	Negative	Negative	Negative

Abbreviation: Ct=cycle threshold; BAL=bronchoalveolar lavage; Jan=January; Feb=February.
* All influenza A-positive samples were negative for H5, H7, and H9 subtypes. Samples with Ct values greater than 35 were considered low viral-load specimens, and full HxNy subtyping or sequencing was not possible for some of these samples because of insufficient viral nucleic acids.

linking human infection to a specific animal source was not available. Therefore, the available epidemiological and laboratory findings suggest a possible swine-associated zoonotic spillover event; however, the exact infection source and transmission route could not be definitively determined.

DISCUSSION

This investigation documented the first confirmed human infection with the influenza A(H1N2)v virus in China. Similar to previous reports from the United States and Europe, human infections with A(H1N2)v have remained rare and have primarily been associated with influenza A viruses of swine origin that cross the species barrier (*6*). Most reported cases present with mild-to-moderate influenza-like illness, and sustained human-to-human transmission has not been documented (*7*). The clinical presentation in the present case was consistent with these observations, further supporting the characterization of A(H1N2)v as a sporadic zoonotic pathogen with limited transmissibility. The key finding of this investigation is that a swine-origin influenza A(H1N2)v virus was detected in a young child through routine ILI surveillance, with whole-genome sequencing supporting a swine-origin reassortant virus and no evidence of secondary human transmission.

Notably, unlike many previously reported A(H1N2)v cases in which direct exposure to swine was identified as a key risk factor (*8*), no direct contact with poultry or livestock was reported in this patient. This finding suggests that indirect or environmental exposure may play a role in the development of infection. Environmental contamination, shared living spaces, and short-distance exposure to animal housing have been proposed as alternative transmission pathways for various influenza viruses, particularly in rural settings where humans and animals coexist in close proximity (*9*). These findings underscore the complexity of exposure assessment in zoonotic influenza investigations. In the present case, pigs and poultry were raised near the residence, and influenza A virus was detected at low viral loads in several pig and environmental samples. These findings support the

possibility of indirect environmental exposure, but do not prove the exact source of infection.

The detection of this case through routine sentinel influenza-like illness (ILI) surveillance highlights the critical role of sensitive surveillance systems and rapid laboratory diagnostics in identifying rare and emerging influenza variants. Previous studies have emphasized that early identification of variant influenza viruses relies heavily on integrated virological surveillance and timely genetic characterization (*10*). In this context, the successful detection and confirmation of A(H1N2)v infection in this case reflect the effectiveness of China's existing influenza surveillance network. Compared with evidence based only on PCR subtyping, whole-genome sequencing provided stronger laboratory evidence for identifying this virus as a swine-origin influenza A(H1N2)v virus.

From a broader public health perspective, this event reinforces the importance of the One Health approach, which integrates the human, animal, and environmental health sectors. Swine populations are important mixing vessels for influenza A viruses, facilitating the reassortment and emergence of novel variants with zoonotic potential. Continuous surveillance in animal populations, particularly swine, combined with data sharing across sectors, is essential for early risk assessment and prevention of future spillover events. The genetic findings in this case were consistent with reassortment among swine influenza virus lineages circulating in China, further supporting the need for coordinated human and animal influenza surveillance.

This investigation has several limitations. First, several influenza A-positive animal and environmental samples had high Ct values, indicating low viral loads. Therefore, full subtyping or sequencing could not be performed on some specimens. Second, because complete viral sequences were not obtained from positive animals or environmental samples, the exact infection source and transmission route could not be confirmed. Third, follow-up respiratory specimens were not collected during treatment or after discharge; therefore, viral shedding was not monitored. Fourth, virus isolation was unsuccessful because of low viral load and/or insufficient viable virus in the residual specimen, limiting further phenotypic and antigenic characterization. Finally, this report described a single sporadic case; therefore, the findings should be interpreted with caution.

Human infection with the influenza A(H1N2)v virus described in this investigation represents a sporadic zoonotic event with no evidence of onward transmission and a limited public health impact. This case is comparable to previously reported A(H1N2)v infections globally, which are characterized by mild illness and the absence of sustained human-to-human spread.

Nevertheless, this finding highlights the ongoing risk posed by variant influenza viruses at the human–animal interface. Strengthened sentinel surveillance, timely epidemiological investigation, enhanced laboratory capacity, and cross-sector collaboration under the One Health framework remain critical for the early detection and mitigation of potential future outbreaks, confirming that human A(H1N2)v infection in China provides important evidence for national influenza surveillance and emphasizes the need to strengthen the genomic monitoring of swine-origin influenza viruses.

Conflicts of interest: No conflicts of interest.

doi: 10.46234/ccdcw2026.149

Corresponding author: Chunrui Luo, yncdclcr@yncdc.cn.

[1] Epidemic Surveillance and Public Health Emergency Response Center, Yunnan Center for Disease Control and Prevention, Kunming City, Yunnan Province, China; [2] Department of Epidemiology, Faculty of Medicine, Prince of Songkla University, Songkhla, Thailand; [3] Institute for Acute Infectious Disease Control and Prevention, Yunnan Center for Disease Control and Prevention, Kunming City, Yunnan Province, China; [4] Surveillance, Early Warning and Emergency Response Center, Zhaotong Center for Disease Control and Prevention, Zhaotong City, Yunnan Province, China; [5] Zhenxiong County Center for Disease Control and Prevention, Zhaotong City, Yunnan Province, China.

Submitted: May 16, 2026
Accepted: July 10, 2026
Issued: July 17, 2026

REFERENCES

1. Chiapponi C, Prosperi A, Moreno A, Baioni L, Faccini S, Manfredi R, et al. Genetic variability among swine influenza viruses in Italy: data analysis of the period 2017-2020. Viruses 2021;14(1):47. https://doi.org/10.3390/v14010047.
2. Whitlow H, Gokool S, Clapp G, Bueno I, Logunleko M, Moore P, et al. Biosecurity uptake and perceived risk of avian influenza among people in contact with birds. Zoonoses Public Health 2026;73(2):152 – 63. https://doi.org/10.1111/zph.70034.
3. Sun HL, Liu HL, Liu YW, Pang ZF, Jiang YL, Liu Q, et al. Genetic characterization of a novel quadruple reassortant influenza A (H1N2) virus from swine, China, 2021. J Infect 2023;86(1):66 – 117. https://doi.org/10.1016/j.jinf.2022.09.009.
4. Klivleyeva N, Glebova T, Saktaganov N, Webby R. Cases of

interspecies transmission of influenza A virus from swine to humans. Vet Sci 2025;12(9):873. https://doi.org/10.3390/vetsci12090873.
5. Centers for Disease Control and Prevention. Novel influenza A virus infections 2024 case definition. 2024 Sep 29. https://ndc.services.cdc.gov/case-definitions/novel-influenza-a-virus-infections/.
6. Chen PW, Jin ZY, Peng LX, Zheng ZY, Cheung YM, Guan J, et al. Characterization of an emergent chicken H3N8 influenza virus in southern China: a potential threat to public health. J Virol 2023;97(6):e00434 – 23. https://doi.org/10.1128/jvi.00434-23.
7. Lanave G, Camero M, Coppola C, Marchi S, Cascone G, Salina F, et al. Serological evidence for circulation of influenza D virus in the ovine population in Italy. Pathogens 2024;13(2):162. https://doi.org/10.3390/pathogens13020162.
8. Kanji JN, Pabbaraju K, Croxen M, Detmer S, Bastien N, Li Y, et al. Characterization of swine influenza A(H1N2) variant, Alberta, Canada, 2020. Emerg Infect Dis 2021;27(12):3045–51. doi:10.3201/eid2712.210298.
9. Jin YF, Cui H, Jiang LN, Zhang C, Li JJ, Cheng HL, et al. Evidence for human infection with avian influenza A(H9N2) virus via environmental transmission inside live poultry market in Xiamen, China. J Med Virol 2023;95(1):e28242. https://doi.org/10.1002/jmv.28242.
10. Yang LY, Zhang T, Han X, Yang J, Sun YX, Ma LB, et al. Influenza epidemic trend surveillance and prediction based on search engine data: deep learning model study. J Med Internet Res 2023;25:e45085. https://doi.org/10.2196/45085.

Methods and Applications

Epidemic Threshold Analysis of an SEIMQR Model Incorporating Healthcare Resource Constraints

Qi Sun[1]; Yu Chang[1,#]

ABSTRACT

Introduction: Epidemic models commonly assume unlimited healthcare resources and overlook a critical operational reality: healthcare system overload reduces recovery rates and amplifies outbreak severity. We propose an enhanced susceptible-exposed-infected-mutant-quarantined-recovered (SEIMQR) model that explicitly links the recovery process to time-varying hospital-bed availability, and thereby better reflects practical healthcare constraints.

Methods: The model integrates a saturating, resource-dependent recovery function and uses the quarantine rate as the primary control parameter. We performed a systematic dynamic analysis using bifurcation theory and validated the model through numerical simulations and empirical coronavirus disease 2019 (COVID-19) surveillance data from the United Kingdom. These data covered distinct phases of the pandemic.

Results: Our analysis identified a precise quarantine threshold (δ = 0.573595) that distinguishes disease elimination from endemic persistence. Simulation results show that strengthening quarantine measures effectively suppresses the epidemic scale. Furthermore, the model fit the reported cumulative case data with high accuracy across different variant-dominant periods and policy regimes, which demonstrates its adaptability.

Conclusion: These findings quantify a critical intervention threshold and illustrate the synergistic relationship between medical capacity and quarantine intensity. This study provides a theoretically grounded, resource-aware framework for guiding integrated public health strategies when healthcare resources are finite. Therefore, it supports more realistic epidemic preparedness and response planning.

The global spread of coronavirus disease 2019 (COVID-19) has placed substantial pressure on public health infrastructure worldwide, underscoring the need for epidemiological models that account for real operational limitations in healthcare systems. Established compartmental models, such as susceptible-exposed-infected-recovered (SEIR), provide a fundamental understanding of transmission dynamics. However, they often assume invariant recovery rates, thereby failing to capture the finite, saturable nature of clinical care resources. In practice, caseload surges exceeding healthcare capacity degrade treatment efficacy, prolong infectious periods, and exacerbate the population disease burden. This creates a nonlinear interaction that must be explicitly incorporated into modeling frameworks. To address these complexities, researchers have developed extended modeling architectures that integrate vaccination and quarantine interventions (*1*), distinguish between hospitalization and community care pathways (*2*), and incorporate behavioral dynamics or fractional-order operators (*3*). Advancing this methodological path, the susceptible-exposed-infected-mutant-quarantined-recovered (SEIMQR) model introduces distinct compartments for variant-specific infections and quarantined individuals, offering a refined structure for simulating transmission dynamics under conditions of viral evolution and targeted intervention (*4*).

A common limitation of existing models is their treatment of recovery rates as static parameters, which may not fully capture the dynamic interaction with concurrent healthcare resource demands. This assumption is particularly restrictive during surge conditions, when system capacity constraints are most acute. To address this gap, this study developed an enhanced SEIMQR framework that incorporates a resource-dependent recovery function, dynamically linking treatment outcomes to available hospital capacity.

The study applies dynamic systems theory and bifurcation analysis, using the quarantine rate as a key bifurcation parameter to investigate how finite healthcare resources, in conjunction with intervention

policies, shape epidemic trajectories. Our analytical approach combines equilibrium stability analysis with numerical validation using longitudinal COVID-19 surveillance data from the United Kingdom. These data encompass distinct pandemic phases marked by dominant variants and evolving policy regimes. By explicitly embedding healthcare resource constraints into the epidemic model, this study aims to advance a more operationally valid framework for informing public health decision-making under conditions of resource scarcity.

METHODS

Model Formulation

The SEIMQR model extends the classical SEIR framework by incorporating compartments for mutant-strain infections and quarantined populations, a structure that fits empirical COVID-19 data better than simpler models. Building on the framework established by Yu et al. (*4*), this model effectively captures variant-driven dynamics and basic intervention effects, providing a solid foundation for further development.

Our refinement addresses a key operational constraint: the dynamic relationship between healthcare system load and patient outcomes. Although the original model effectively captures variant dynamics and intervention effects, it, like many compartmental approaches, treats the recovery rate as a constant parameter, independent of the scale of infections. This formulation does not account for the degradation of treatment efficacy that occurs when healthcare systems approach or exceed their operational capacity. In practice, finite resources, such as hospital beds, staffing, and equipment impose an upper limit on medical throughput. As the infected population grows, the per-capita recovery rate declines, becoming state-dependent rather than constant. The absence of this feedback mechanism limits the model's ability to reflect how medical capacity influences equilibrium states and epidemic thresholds.

To capture this saturation effect, we formulate a resource-dependent recovery function that characterizes the dynamic relationship between healthcare capacity and disease progression. The function takes the form of (*5*):

$$\varepsilon(b, I) = \varepsilon_0 + (\varepsilon_1 - \varepsilon_0)\frac{b}{I + b} \quad (1)$$

where b denotes the normalized number of hospital beds (serving as a proxy for healthcare resources), I is the symptomatic infected fraction, and ε_1 and ε_0 are the attainable recovery rates under sufficient resources and extreme overloads, respectively.

This functional form captures the saturation of medical capacity as the infected population grows, thereby introducing state-dependent feedback into the recovery process. By integrating this mechanism and treating the quarantine rate as a bifurcation parameter, the modified model enables systematic investigation of how finite healthcare resources reshape the system's dynamic landscape, offering a more realistic foundation for assessing public health strategies under resource-constrained scenarios. A dynamic flow diagram of the modified SEIMQR model is shown in Figure 1.

This enhancement yields the modified SEIMQR system:

$$\begin{cases} \frac{dS}{dt} = \mu - \alpha S(I+E) - \eta SM - \mu S \\ \frac{dE}{dt} = \alpha S(I+E) + \eta SM - \beta E - \delta E - \mu E \\ \frac{dI}{dt} = \frac{1}{2}\beta E - \gamma I - \delta I - \left(\varepsilon_0 + (\varepsilon_1 - \varepsilon_0)\frac{b}{I+b}\right) I - \mu I \\ \frac{dM}{dt} = \frac{1}{2}\beta E + \gamma I - \left(\varepsilon_0 + (\varepsilon_1 - \varepsilon_0)\frac{b}{I+b}\right) M - \delta M - \mu M \\ \frac{dQ}{dt} = \delta(E + I + M) - \mu Q \\ \frac{dR}{dt} = \left(\varepsilon_0 + (\varepsilon_1 - \varepsilon_0)\frac{b}{I+b}\right) I \\ + \left(\varepsilon_0 + (\varepsilon_1 - \varepsilon_0)\frac{b}{I+b}\right) M - \mu R \end{cases} \quad (2)$$

where $S(t)$, $E(t)$, $I(t)$, $M(t)$, $Q(t)$, $R(t)$ denote the proportions of the susceptible, exposed, symptomatic infected, mutant-strain infected, quarantined, and recovered populations, respectively, satisfying the normalization constraint $S + E + I + M + Q + R = 1$. The parameter μ denotes the natural birth and death rate. The coefficients $\alpha$and η represent the transmission probabilities associated with contacts between susceptible individuals and the symptomatic infected/exposed classes and mutant-strain infectives, respectively. The parameter β governs the transition from exposed to infectives, while δ measures the quarantine intensity applied to exposed individuals. The mutation probability γ characterizes the conversion from the symptomatic infected class to the mutant-strain infected class.

Let $X(t) = (E, I, M)^T$. Then, we have $\frac{dX}{dt} = F - V$, where

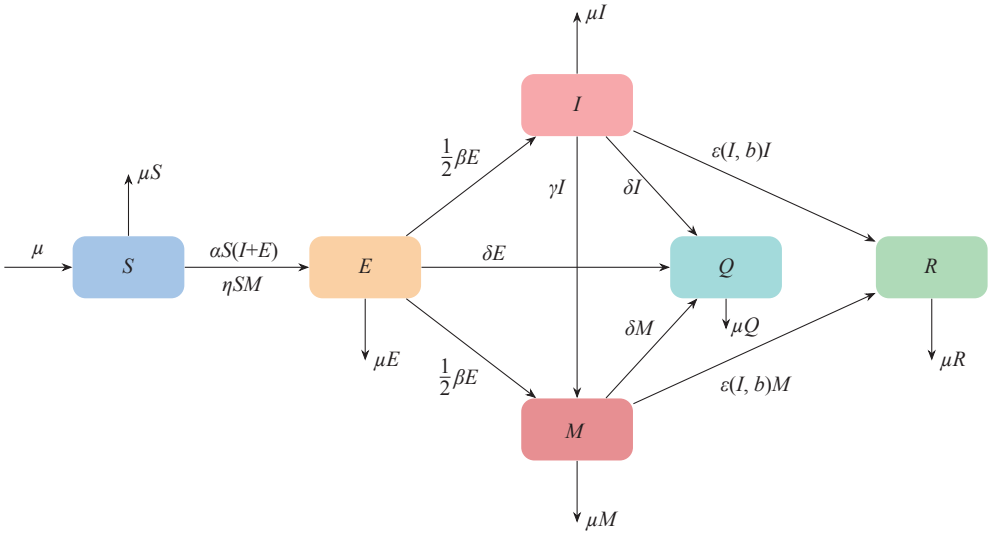

FIGURE 1. State-transition diagram of the modified SEIMQR model.
Abbreviation: SEIMQR=susceptible-exposed-infected-mutant-quarantined-recovered.

$$F = \begin{bmatrix} \alpha S(I+E) + \eta SM \\ 0 \\ 0 \end{bmatrix},$$

$$V = \begin{bmatrix} \beta E + \delta E + \mu E \\ \gamma I + \delta I + \left(\varepsilon_0 + (\varepsilon_1 - \varepsilon_0)\dfrac{b}{I+b}\right) I + \mu I - \dfrac{1}{2}\beta E \\ \left(\varepsilon_0 + (\varepsilon_1 - \varepsilon_0)\dfrac{b}{I+b}\right) M + \delta M + \mu M - \dfrac{1}{2}\beta E - \gamma I \end{bmatrix}. \quad (3)$$

Upon evaluating F and V at the disease-free equilibrium E_0, the corresponding Jacobian matrices are obtained as

$$J_F = \begin{bmatrix} \alpha & \alpha & \eta \\ 0 & 0 & 0 \\ 0 & 0 & 0 \end{bmatrix},$$

$$J_V = \begin{bmatrix} \beta + \delta + \mu & 0 & 0 \\ -\dfrac{\beta}{2} & \gamma + \delta + \varepsilon_1 + \mu & 0 \\ -\dfrac{\beta}{2} & -\gamma & \delta + \varepsilon_1 + \mu \end{bmatrix}. \quad (4)$$

The basic reproduction number R_0 is defined as the spectral radius of the next-generation matrix $J_F J_V^{-1}$, evaluated at the disease-free equilibrium E_0. Therefore, R_0 is given by

$$\rho\left(J_F J_V^{-1}\right) = \frac{\alpha}{\beta + \delta + \mu} + \frac{\alpha\beta}{2(\beta + \delta + \mu)(\gamma + \delta + \mu + \varepsilon_1)} + \frac{\eta\beta(2\gamma + \delta + \mu + \varepsilon_1)}{2(\beta + \delta + \mu)(\gamma + \delta + \mu + \varepsilon_1)(\delta + \mu + \varepsilon_1)} \quad (5)$$

where $\rho(\cdot)$ denotes the spectral radius.

Parameter Estimation

The particle swarm optimization (PSO) algorithm was employed to explore the parameter space and identify the parameters set that minimized the discrepancy between the model outputs and the observed data. In this study, the cumulative number of confirmed cases served as the fitting target, and goodness-of-fit was quantified using the root mean square error (RMSE) as the objective function. Owing to its efficient convergence and robust global search capability, PSO is particularly well-suited for parameter estimation in nonlinear dynamical systems with multiple parameters.

Data Source

COVID-19 cumulative case data were obtained from a worldwide dataset (*6*). The data include daily cumulative confirmed cases for the United Kingdom across three distinct pandemic phases: Phase 1 (Delta-dominant, June 1 to July 15, 2021), Phase 2 (emergence of the Omicron variant, December 20, 2021, to January 20, 2022), and Phase 3 ("living with the virus" policy, April 15 to May 31, 2022). Based on the same data source, the total population of the United Kingdom in 2021 was 67,326,569.

RESULTS

We performed an integrated theoretical and numerical analysis of how the quarantine rate influences epidemic outcomes within the modified SEIMQR model. The quarantine rate was selected as the primary control parameter due to system complexity.

The model consistently admitted a disease-free equilibrium (DFE) under all parameter configurations. However, its practical attainability depends critically on the quarantine rate. When the quarantine rate is low, sustained transmission leads to infected population persisting at nonzero levels, a pattern characteristic of an endemic state. As the rate increases, a critical threshold is reached beyond which sustained transmission cannot be maintained.

Numerical simulations were conducted with the following fixed values: $\mu = 0.1, \alpha = 0.82, \eta = 0.7, \beta = 0.3, \gamma = 0.15, \varepsilon_1 = 0.8, \varepsilon_0 = 0.01, \ b = 0.5$, while the quarantine rate was systematically varied.

Figure 2 shows the system's bifurcation behavior with respect to the quarantine rate δ. For $0 < \delta < 0.573595$, the disease-free state is unstable and a stable endemic state exists, with infected compartments converging to nonzero steady-state levels. At the transcritical bifurcation (TB) value $\delta = 0.573595$, the endemic and disease-free states coincide, marking a threshold transition. For $0.573595 < \delta < 1$, the endemic state disappears and the disease-free state becomes stable, indicating effective epidemic control.

Figure 3 illustrates the synergistic effect of healthcare capacity b and quarantine rate δ on the equilibrium infected proportion I^*. The results confirm that although b does not influence R_0 or the transcritical bifurcation threshold, it strongly modulates the endemic infection level once δ falls below the threshold; this effect becomes more pronounced as the quarantine weakens. In the extinction regime ($0.573595 < \delta < 1$ and $R_0 < 1$), I^* remains at zero and is insensitive to b. In the endemic regime ($0 < \delta < 0.573595$ and $R_0 > 1$), I^* becomes highly responsive to b, with a marked increase in sensitivity as δ decreased.

For empirical validation, we estimated time-varying parameters using particle swarm optimization, fitting COVID-19 cumulative case data from the United Kingdom across three distinct pandemic phases and

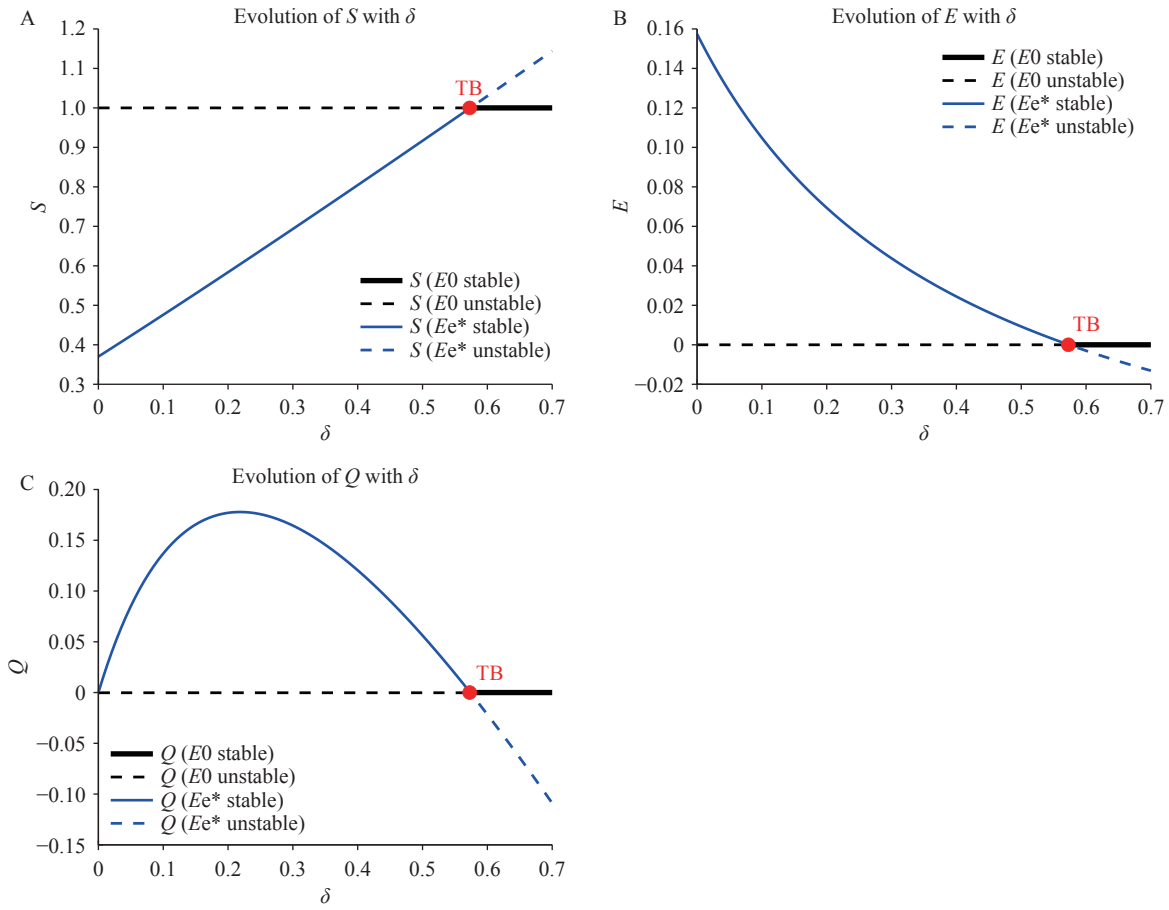

FIGURE 2. Bifurcation diagrams. (A) The quarantine rate δ — Susceptible (S); (B) The quarantine rate δ — Exposed (E); (C) The quarantine rate δ — Quarantined (Q).
Abbreviation: TB=transcritical bifurcation.

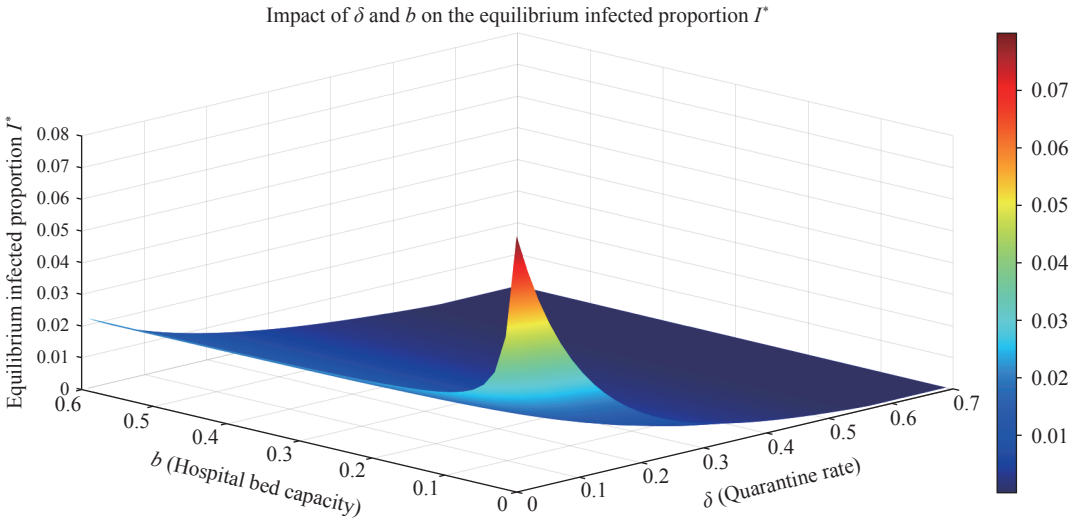

FIGURE 3. Impact of b and δ on the equilibrium infected proportion I^*.

drawing on the organisation for economic co-operation and development (OECD) report *Health at a Glance: Europe 2024* (*7*). Figure 4 shows the fitted cumulative case curves alongside reported data. During the Delta-variant-dominant phase (June 1–July 15, 2021), the model achieved a mean absolute percentage error (MAPE) of 0.11%. During the Omicron emergence period (December 20, 2021–January 20, 2022), the estimated mutant strain transmission rate increased to 0.64, while the quarantine rate decreased to 0.034, successfully capturing the variant's heightened transmissibility and reduced controllability. Under the "living with the virus" policy (April 15–May 31, 2022), the quarantine rate further declined to 0.0085, and the model effectively reproduced the associated increase in infection risk with a MAPE of 0.05%. The fitted parameters, initial conditions, and corresponding basic reproduction numbers R_0 are summarized in Table 1; the coefficients of determination for Figure 4A–C were $R^2 = 0.9993$, $R^2 = 0.9989$ and $R^2 = 0.9913$, respectively. These results confirm that the modified SEIMQR framework can be adapted to diverse epidemiological contexts and policy regimes, accurately capturing shifts in transmission dynamics driven by emerging variants and changes in intervention intensity.

DISCUSSION

This study presents an enhanced SEIMQR modeling framework that explicitly incorporates healthcare capacity constraints, addressing notable limitations of conventional compartmental models. A dynamic, resource-dependent recovery function, $\varepsilon(b, I)$ captures the impact of healthcare system strain on individual patient outcomes and population-level epidemic dynamics. This function $\varepsilon(b, I)$ links the recovery rate to the infected population size: when infections are few, healthcare resources are abundant and the recovery rate approaches its upper bound; as infection grows and the system saturates, the recovery rate declines, prolonging infectious periods and amplifying transmission. Traditional fixed-recovery-rate models cannot capture this feedback.

Theoretical analysis revealed that near the transcritical bifurcation, the system exhibits extreme sensitivity to initial conditions. Minimal differences in the initial infected proportion or model parameters can be amplified by nonlinear mechanisms, causing distinctly different epidemic pathways. From a nonlinear dynamics perspective, this divergence under critical conditions is directly linked to the bifurcation-induced topological change in system stability. This underscores the pivotal regulatory role of the quarantine rate in epidemic transmission dynamics.

Validation against longitudinal COVID-19 data from the United Kingdom demonstrated the model's adaptability across diverse epidemiological contexts, including periods dominated by distinct variants and varying policy interventions. These results highlight the importance of integrating empirical healthcare resource limitations into epidemic forecasting, especially when healthcare system saturation can delay control efforts and prolong community transmission.

Consistent with our findings, identifying a precise

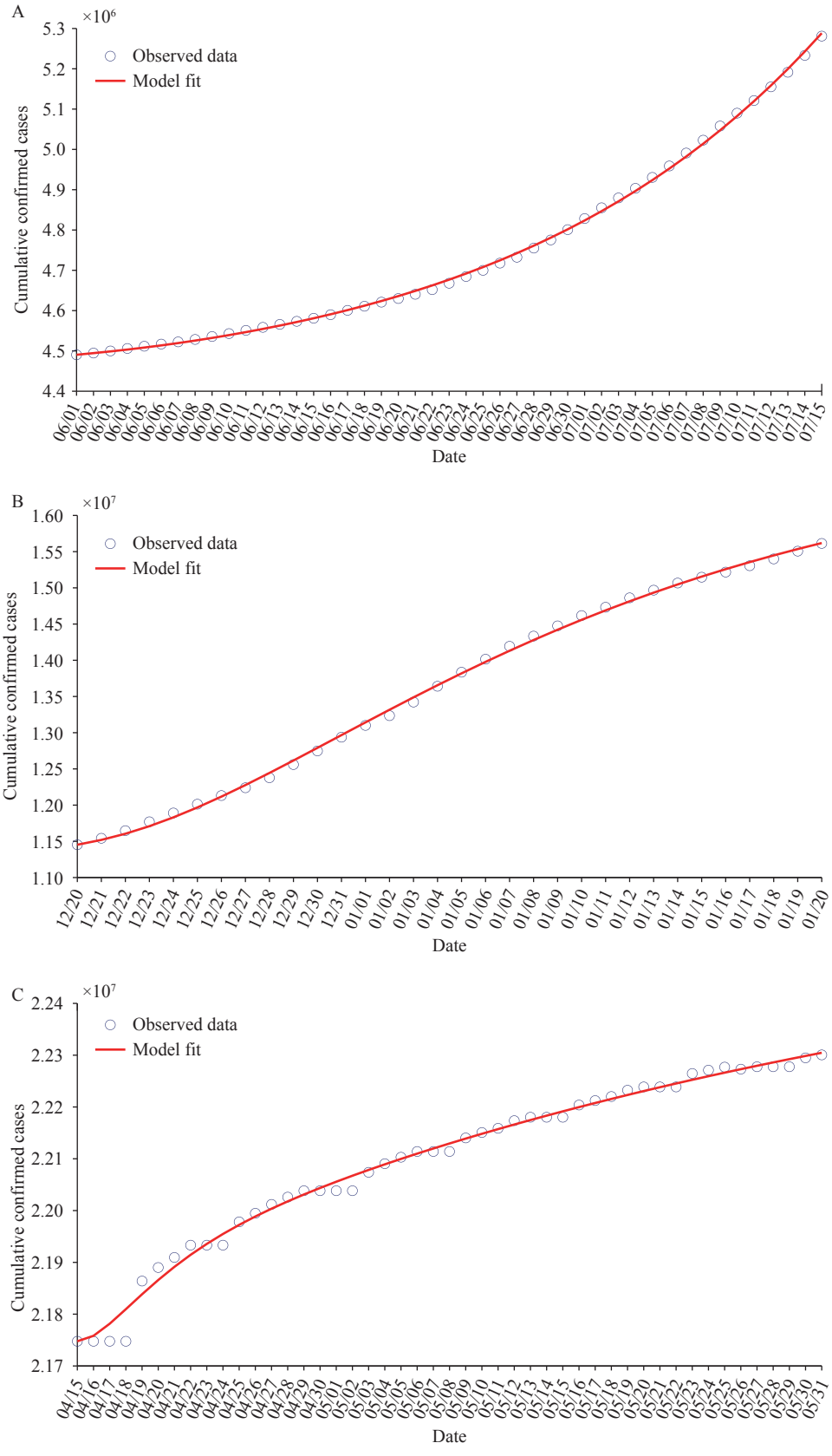

FIGURE 4. Model-fitted cumulative confirmed COVID-19 cases in the United Kingdom across three representative periods. (A) 1 June–15 July 2021, (B) 20 December 2021–20 January 2022, and (C) 15 April–31 May 2022.
Abbreviation: COVID-19=coronavirus disease 2019.

TABLE 1. Model parameters, R_0 and initial values across three distinct pandemic phases in the United Kingdom.

Phase	Parameter	Value	Source	Parameter	Value	Source
1	μ	0.00001094	(6)	γ	0.10158413	Fitting
	α	0.12530421	Fitting	ε_1	0.01398170	Fitting
	η	0.26454923	Fitting	ε_0	0.01051092	Fitting
	β	0.67564826	Fitting	b	0.00225051	Fitting
	δ	0.11270636	Fitting	R_0	1.68704179	Calculated
	$S(0)$	$E(0)$	$I(0)$	$M(0)$	$Q(0)$	$R(0)$
	0.88649523	0.00008944	0.00051128	0.00000094	0.00000094	0.11290217
2	μ	0.00001094	(6)	γ	0.03684764	Fitting
	α	0.05825147	Fitting	ε_1	0.09273017	Fitting
	η	0.64340215	Fitting	ε_0	0.04368076	Fitting
	β	0.45728898	Fitting	b	0.00200918	Fitting
	δ	0.03369863	Fitting	R_0	3.18912013	Calculated
	$S(0)$	$E(0)$	$I(0)$	$M(0)$	$Q(0)$	$R(0)$
	0.13935162	0.00188082	0.17271673	0.00000036	0.33032572	0.35572475
3	μ	0.00001094	(6)	γ	0.25964701	Fitting
	α	0.65734363	Fitting	ε_1	0.01203041	Fitting
	η	0.15883262	Fitting	ε_0	0.00846606	Fitting
	β	0.50308248	Fitting	b	0.00192497	Fitting
	δ	0.00847932	Fitting	R_0	9.77151472	Calculated
	$S(0)$	$E(0)$	$I(0)$	$M(0)$	$Q(0)$	$R(0)$
	0.03477658	0.00000047	0.03397416	0.00166396	0.46440994	0.46517489

Note: $S(0)$ is the initial proportion of the susceptible population. $E(0)$ is the initial proportion of the exposed population. $I(0)$ is the initial proportion of the symptomatic infected population. $M(0)$ is the initial proportion of the mutant-strain infected population. $Q(0)$ is the initial proportion of the quarantined population. $R(0)$ is the initial proportion of the recovered population. R_0 is the basic reproduction number.

quarantine threshold provides evidence-based guidance for containment strategies in resource-limited settings. The transcritical bifurcation value serves as a clear operational target; control measures should be dynamically calibrated to sustain it. Where such intensity is unattainable, our analysis shows that expanding healthcare capacity b is essential to mitigate the long-term infection burden. Furthermore, the model elucidates key synergies between healthcare resource availability and quarantine effectiveness. As healthcare systems approach saturation, strengthening quarantine alone may yield diminishing returns. Coordinated interventions combining temporary healthcare expansion with targeted quarantine offer superior outcomes compared with single-component approaches.

Although this model advances the understanding of resource-constrained epidemic dynamics, it has several limitations. The current framework does not account for spatial heterogeneity in transmission and healthcare access, dynamic behavioral adaptations, or the evolving effects of vaccination and population immunity. Future research should incorporate these elements to develop more comprehensive models for complex, practical public health challenges.

Collectively, this study establishes a practical resource-aware modeling framework directly linking healthcare constraints to intervention planning. By providing decision-makers a more realistic scenario-evaluation tool, it contributes to improved epidemic preparedness and response in resource-limited environments.

Conflicts of interest: No conflicts of interest.

doi: 10.46234/ccdcw2026.150

Corresponding author: Yu Chang, changyu@mail.buct.edu.cn.

[1] College of Mathematics and Physics, Beijing University of Chemical Technology, Beijing, China.

Submitted: March 16, 2026
Accepted: July 10, 2026
Issued: July 17, 2026

REFERENCES

1. Annas S, Pratama MI, Rifandi M, Sanusi W, Side S. Stability analysis and numerical simulation of SEIR model for pandemic COVID-19 spread in Indonesia. Chaos Solitons Fractals 2020;139:110072. https://doi.org/10.1016/j.chaos.2020.110072.
2. He SB, Peng YX, Sun KH. SEIR modeling of the COVID-19 and its dynamics. Nonlinear Dyn 2020;101(3):1667 – 80. https://doi.org/10.1007/s11071-020-05743-y.
3. Joshi H, Yavuz M, Townley S, Jha BK. Stability analysis of a non-singular fractional-order covid-19 model with nonlinear incidence and treatment rate. Phys Scr 2023;98(4):045216. https://doi.org/10.1088/1402-4896/acbe7a.
4. Yu ZH, Zhang JM, Zhang Y, Cong XY, Li XB, Mostafa AM. Mathematical modeling and simulation for COVID-19 with mutant and quarantined strategy. Chaos Solitons Fractals 2024;181:114656. https://doi.org/10.1016/j.chaos.2024.114656.
5. Shan CH, Zhu HP. Bifurcations and complex dynamics of an SIR model with the impact of the number of hospital beds. J Differ Equations 2014;257(5):1662 – 88. https://doi.org/10.1016/j.jde.2014.05.030.
6. Mathieu E, Ritchie H, Rodés-Guirao L, Appel C, Gavrilov D, Giattino C, et al. COVID-19 pandemic. 2020. https://ourworldindata.org/coronavirus. [2024-7-18].
7. OECD. Health at a glance: Europe 2024: state of health in the EU cycle. OECD Publishing. 2024. http://dx.doi.org/10.1787/b3704e14-en. [2024-11-18].

Youth Editorial Board

Indexed by Science Citation Index Expanded (SCIE), Social Sciences Citation Index (SSCI), PubMed Central (PMC), Scopus, Chinese Scientific and Technical Papers and Citations, and Chinese Science Citation Database (CSCD)

The inauguration of *China CDC Weekly* is in part supported by Project for Enhancing International Impact of China STM Journals Category D (PIIJ2-D-04-(2018)) of China Association for Science and Technology (CAST).

CHINA CDC WEEKLY

CCDC weekly

Vol. 8 No. 29 Jul. 17, 2026

中国疾病预防控制中心周报(英文)

Responsible Authority
National Disease Control and Prevention Administration

Sponsor
Chinese Center for Disease Control and Prevention &
Chinese Academy of Preventive Medicine

Editor-in-Chief
Jianwei Wang

Editing and Publishing
China CDC Weekly Editorial Office
No.155 Changbai Road, Changping District, Beijing, China
Tel: 86-10-63150501, 63150701
Email: weekly@chinacdc.cn

Printing: Beijing Kexin Printing Co., Ltd

Complimentary Access

CSSN
ISSN 2096-7071 (Print)
ISSN 2097-3101 (Online)
CN 10-1629/R1